Quantification on fuel cell degradation and techno-economic analysis of a hydrogen-based grid-interactive residential energy sharing network with fuel-cell-powered vehicles

Yingdong He[1, 2], Yuekuan Zhou[2, *] , Zhe Wang[3], Jia Liu[4], Zhengxuan Liu[2], Guoqiang Zhang[2]

[1]*Center for the Built Environment, University of California, Berkeley, Berkeley, California, U.S.A.*
[2]*College of Civil Engineering, National Center for International Research Collaboration in Building Safety and Environment, Hunan University, Changsha, Hunan, China*
[3] *Building Technology and Urban Systems Division, Lawrence Berkeley National Laboratory, Berkeley, CA, U.S.A.*
[4] *Department of Building Services Engineering, Faculty of Construction and Environment, Hong Kong Polytechnic University, Kowloon, Hong Kong, China*

Abstract: Hydrogen-based (H_2-based) interactive energy networks for buildings and transportations provide novel solutions for carbon-neutrality transition, regional energy flexibility and independence on fossil fuel consumption, where vehicle fuel cells are key components for H_2-electricity conversion and clean power supply. However, due to the complexity in thermodynamic working environments and frequent on/off operations, the proton exchange membrane fuel cells (PEMFCs) suffer from performance degradation, depending on cabin heat balance and power requirements, and the ignorance of the degradation may lead to the performance overestimation. In order to quantify fuel cell degradation in both daily cruise and vehicle-to-grid (V2G) interactions, this study firstly proposes a two-space cabin thermal model to quantify the ambient temperature of vehicle PEMFCs and the power supply from PEMFCs to vehicle HVAC systems. Afterwards, a stack voltage model is proposed to quantify the fuel cell degradation for multiple purposes, such as daily transportation and V2G interactions. Afterwards, the two models are coupled in a community-level based building-vehicle energy network, consisting of twenty single residential buildings, rooftop PV systems, four hydrogen vehicles (HVs), a H_2 station, community-served micro power grid, local main power grid, and local H_2 pipelines, located in California, U.S.A. Comparative analysis with and without fuel cell degradation is conducted to study the impact of dynamic fuel cell degradation on the energy flexibility and operating cost. Furthermore, a parametrical analysis is conducted on the integrated HV quantity and the grid feed-in tariff to reach trade-off strategies between associated fuel cell degradation costs and grid import cost savings. The results indicate that, in the proposed hydrogen-based building-vehicle energy network, the total fuel cell degradation is 3.16% per vehicle within one year, where 2.50% and 0.66% are caused by daily transportation and V2G interactions, respectively. Furthermore, in the H_2-based residential community, the total fuel cell degradation cost is US$6945.2, accounting for 33.4% of the total operating cost at $20770.61. The sensitivity analysis results showed that, when the HV quantity increases to twenty, the fuel cell degradation of each HV decreases to 2.50%, whereas the total fuel cell degradation cost increases to 42.8% of the total operating cost. Last but not the least, the cost saving by V2G interactions can compensate the fuel cell degradation cost when the grid feed-in tariff is reduced by 40%. Research results can provide basic modelling tools on dynamic fuel cell degradation, in respect to vehicle power supply, vehicle HVAC and V2G interactions, together with techno-economic feasibility analysis, paving path for the development of hydrogen energy for the carbon-neutrality transition.

Keywords: Solar Energy; Wind Turbine; Fuel cell degradation; Cabin thermal model; Hydrogen Energy Storage and Economy; Distributed Hydrogen Infrastructure.

Graphical abstract:

Corresponding author: Tel.: (+852) 2766 4560
Email: yuekuan.zhou@connect.polyu.hk
yuekuan.zhou@outlook.com (Zhou Y.)

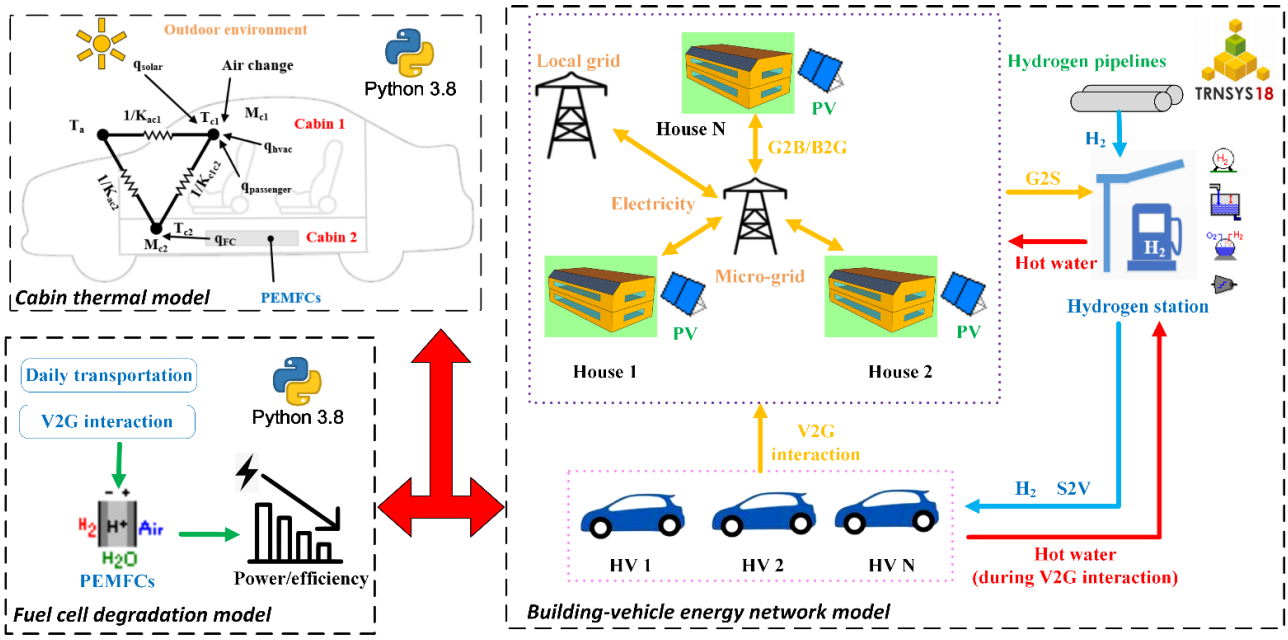

https://doi.org/10.1016/j.apenergy.2021.117444
https://escholarship.org/uc/item/8ms2x24r

1 Introduction

1. Background

Buildings and vehicles account for the largest share of total energy consumption for meeting people's living needs (such as energy use for space cooling in summer [1, 2] and space heating in winter [3]) and supporting daily travelling activities [4, 5]. In the U.S.A., buildings and vehicles consume 28% and 37% of the total end-use energy, respectively [6]. In Europe, buildings and vehicles consume 60% of the total energy consumptions [7]. The considerable amount of energy consumption in buildings and vehicles causes a heavy burden on current energy infrastructures (e.g., power grid and vehicle refilling stations) with power damage and power failure, together with energy shortage crisis and global warming due to the over-used fossil fuels.

Due to the high energy density and clean by-product of water, hydrogen energy systems are promising and the deployment of hydrogen-based (H_2-based) building-vehicle energy networks is critical to enhance regional energy flexibility and reduce the reliance on fossil fuels. Specifically, H_2-based building-vehicle energy networks can be deployed in office buildings [8], single residential houses [9], and even communities with different building types [10, 11]. In recent years, due to the environmental friendliness and sustainability, H_2 energy technologies, infrastructures, and market are under fast development [12]. Fuel-cell-driven hydrogen vehicles (FCHVs, in short, HVs), as one of the typical commercial H_2 energy products, have been well-designed and promoted by many famous commercial companies like Toyota [13] and Honda [14]. Unlike traditional fossil fuels which produce multiple pollutants, H_2 energy has little pollution since the byproduct is water. H_2 energy also has high sustainability since it can be produced through the electrolysis process with electricity from renewable energy systems, such as solar photovoltaic (PV) systems and wind turbines [15, 16]. The integration of the HVs with regional communities, forming interactive building-vehicle energy networks with distributed renewable systems, can not only cover building energy demands, but also produce H_2 for energy storage. The stored onsite-renewable-generated H_2 can be used to charge HVs for daily transportation or be reversely converted into electricity by proton exchange membrane fuel cells (PEMFCs) of HVs for powering buildings. Compared to building-vehicle-isolated networks which strongly rely on the local power grid, building-vehicle-integrated energy networks with H_2 production and storage reduces both the independence of buildings on local power grid and the fossil fuel consumption by vehicles, which enhances regional grid stability, energy flexibility, and carbon neutralization [17, 18]. Moreover, compared to normal oil-fueled vehicles, in regional building-vehicle energy networks, HVs not only act as an energy consumer, but also an energy storer (H_2 stored in vehicle tanks) and backup power unit (PEMFCs as power suppliers for buildings or electric grid) for regional energy systems. The positive effects of H_2 energy infrastructures and HVs on regional energy systems will motivate and attract more stakeholders (building owners, vehicle owners, electric power companies, H_2 gas companies, governments, and more) to promote the development and application of clean and sustainable energy.

Recently, exploiting and quantifying the benefits of H_2-energy-based building-vehicle energy networks are gaining popularity in the academia. Mehrjerdi et al. [19] designed a building-vehicle energy network integrating a single house, PV panels, wind turbines, an electrolyzer, and HVs. They pointed out that, if the traditional oil-fueled vehicles can be replaced by HVs, and the distributed renewable systems can support onsite H_2 production, more than 10% of the total energy use of the building-vehicle network can be reduced. Cao and Alanne [20] established a building-vehicle network consisting of a residential house, PV panels, wind turbines, an electrolyzer, and a HV. They found that deploying 8-kW wind turbines or 12-kW PV panels can actualize the net-zero energy use for the whole energy network. Similarly, Farahani et al. [8] proposed a H_2-supported building-vehicle energy network, which integrates an office building, battery-driven electrical vehicles (EVs), and HVs, with wind turbines and PV panels. They claimed that the energy network can be 100% supported by renewable energy through the onsite renewable energy production and energy

storage by vehicles. In order to actualize regional energy flexibility and grid stability, Sahu et al. [21] studied the possibility of integrating 1000 residential houses and 500 HVs with vehicle-to-grid (V2G) interaction. The results showed that 80% of the building energy demand can be covered by renewable systems rather than by the local grid. The HVs play significant roles in relieving the pressure of regional power grids. Maroufmashat et al. [22] established a mathematical model for optimal planning and operation of H_2-based micro-grids for communities. They found that the distributed H_2 generation is more economic and environmental-friendly than the H_2 delivery. Mukherjee et al. [23] proposed a renewable H_2-based powered micro-grid design for a community integrated with PV systems, wind turbines, electrolyzers, H_2 tanks, and HVS, in Canada. With the H_2-storage, the micro-grid can provide backup electricity and support the community for two days after being disconnected from the local power grid. Felgenhauer et al. [24] investigated a building-vehicle energy network consisting of 8000 houses, HVs, and distributed renewable systems located in California, U.S.A. They found that 80% of the H_2 for transportation was produced by renewable electricity, which contributed to reducing more than 40% of the regional carbon emission as compared to the case with oil-fueled vehicles. Oldenbroek et al. [25] investigated a city-scale building-vehicle energy network which integrates residential houses, H_2 stations, and HVs. The network is supported by distributed PV systems and wind turbines in the city. Due to the high penetration of renewable energy into the building and transportation sectors, the whole energy network realizes low energy costs for buildings (0.09 €/kWh) and HVs (0.02 €/km). After reviewing more than 100 existing studies, Lin et al. [26] pointed out that H_2-based smart grid is gaining popularity and the society is moving towards a H_2-supported future. But the H_2-based grid is still faced with many technical problems, including long-term H_2 storage and energy management strategies.

The enormous potential benefits of H_2-supported building-vehicle energy networks in enhancing regional energy flexibility and reducing environmental pollution, have attracted the attention of researchers, entrepreneurs, and government officers, promoting the development of H_2 infrastructures and commercial products. For example, in 2020, the U.S.A. proposed an ambitious plan, i.e., *Road Map to a Hydrogen Economy*, to stimulate its national-wide H_2 energy development and application [27]. One of this plan's medium-term goals it to enhance clean H_2 energy application in the transportation sector, aiming to sell at least one million commercial HVs and build at least 5000 H_2 stations in the U.S.A. by 2030. One of this plan's long-term goals is to actualize clean H_2 energy supporting 14% of the national end-use energy of the U.S.A. by 2050, providing 4, 8, and 27 million tons of H_2 for supporting power grid regulation, buildings, and vehicles, respectively. This plan will finally formulate a comprehensive H_2 energy network, systematically connecting industries, buildings, and vehicles. The H_2 energy network will become the second most important network following the current grid network.

Within local H_2-supported building-vehicle energy networks, vehicle PEMFC is the key component which actualizes the H_2-electricity conversion for supporting transportation and covering building energy shortage. PEMFCs are widely used due to the high power density, moderate operating temperature (60 - 80°C), and strong resistance to corrosion compared to other types of fuel cells [28]. Nonetheless, a common issue of vehicle PEMFCs is the performance degradation (namely, the fuel cell degradation). To be specific, in practice, after a long-time use, the components of PEMFCs, such as the membrane, electrodes, sealing gasket, and more, will have different degrees of degradation due to mechanical, thermal, chemical, electrochemical, and structural failures [29]. As a result, the energy efficiency of PEMFCs will decrease over time. When the fuel cell degradation increases to a certain level, vehicles' PEMFCs need to be replaced [30], which causes the additional operating cost of the vehicles (namely, the fuel cell degradation cost). Previous studies have proposed some theoretical or semi-empirical methods to quantify the vehicle fuel cell degradation. For example, electrochemical impedance spectrometry (EIS) is widely used in fuel cell performance diagnosis due to its simply non-invasive approach [31]. Specifically, EIS imposes special-designed electrical

disturbance on the diagnosed fuel cell to test its response and perturbation. Different levels of fuel cell degradation as well as their operation conditions will produce different spectrum shapes, which reflect the fuel cell performance changes [32]. In practice, EIS adopts scaling-up technique which simulates the impedance of a full stack but only needs to test a single cell or part of a full stack [33]: the actual experimental data of a single cell or part of a full stack is extended by adopting physical reasoning and phenomenological modelling. Thus, EIS can significantly simplify the test process of fuel cells and lower the testing cost. Meanwhile, the fuel cell degradation can be also estimated through some data-driven models such as echo-state networks [34] and adaptive neuro-fuzzy inference systems [35]. The data-driven models are robust for predicting fuel cell degradation since they are built with the data from practical fuel cell operations. It should be noted that the EIS estimation and the data-driven models are hard to be widely applied in dynamic calculation or simulation of fuel cell degradation, since abundant onsite-measured data is required with cost-worthy, time-consuming, and labor-intensive characteristics.

Stack voltage degradation model [30] provides an easy-to-implement method for predicting fuel cell degradation, which correlates fuel cell degradation to the output power of fuel cells. In practice, the most significant performance change of fuel cells is the stack voltage drop [36], and it mainly brings two main effects: (1) the decreased maximum output power for driving vehicle motors and supporting other energy consumers like buildings under vehicle-to-building interaction [30], and (2) the decreased energy efficiency, which means the decreased output power with the same H_2 consumption rate of fuel cells [37]. Using the stack voltage degradation can directly quantify the fuel cell performance change. Besides, the stack voltage drop model calculates the fuel cell degradation (the stack voltage drop) by using output power parameters, i.e., the large load changing cycles, start-stop cycles, idling time, and maximum power time, which can be easily obtained through theoretical calculations or onsite measurement. Although the stack voltage degradation model is semi-empirical, it provides a practical way to quantify the fuel cell degradation with easy-to-measure parameters. Nonetheless, since the fuel cell degradation models in current academia are only for evaluating the lifetime of PEMFCs serving daily transportation only, more investigations are needed to quantify the fuel cell degradation when being applied in dynamic energy interactions of interactive building-vehicle energy networks.

1.2 Scientific gaps

The literature review above indicates that integrating buildings, HVs, and H_2 systems can enhance regional energy flexibility and grid stability, in respect to the intermittent renewable power supply, diversity and randomness of district energy demands. PEMFC is a key energy conversion component in building-vehicle energy networks, and the dynamic degradation has significant effects on the energy-efficiency and cost of the networks. Nonetheless, some critical issues still remain unclear:

(1) vehicles' fuel cell degradation is common in practice, and it leads to reductions in both the PEMFCs' maximum output power and H_2-electricity conversion efficiency [30], together with the increase in energy operating cost. Considering that the economic costs of vehicles' PEMFCs are still high (e.g., PEMFCs are $11000 for each Toyota HV [38]), the fuel cell degradation cost should not be ignored, which will otherwise lead to the overestimation on techno-economic performance. Furthermore, some models, such as that in reference [30], have been proposed to evaluate PEMFCs' degradation but only for transportation applications. The quantification on dynamic HVs' fuel cell degradations in building-vehicle energy networks with V2G interactions, is still rare in the academia.

(2) since vehicle PEMFCs are installed in cabin spaces, the cabin indoor temperature affects PEMFCs' heat balance which dominates PEMFCs' heat released to the ambient cabin environment and PEMFCs' thermal management system. The cabin indoor temperature also affects vehicles' electrical energy balance which dominates the additional energy from vehicle PEMFCs to support vehicle heating, ventilation, and air conditioning (HVAC)

systems for maintaining comfortable cabin environments. Therefore, the cabin thermal environment of HVs affects the energy consumption of vehicle PEMFCs as well as the fuel cell degradation. However, few relevant studies study the effects of cabin thermal environments on the thermodynamic and energy performances in building-vehicle energy networks.

(3) with the ambitious goal of H_2 infrastructure development of the U.S.A [27], HVs are expected to gain popularity in the near future, and a large amount of HVs will emerge in local communities. On the one hand, more HVs in a community can provide V2G services for covering building energy demand, which helps enhance grid stability and reduce each HV's V2G-caused fuel cell degradation. On the other hand, more HVs need more energy for daily transportation and thus lead to a higher total fuel cell degradation (including both transportation and V2G interactions). The fuel cell degradation with the increased HV quantity will significantly affect the energy flexibility and energy operating cost of a local community, but this issue is usually ignored in the existing studies.

(4) with the rapid increase of installed renewable capacity, the world is experiencing a decreasing price of distributed renewable electricity [39], and the declining economic earning will inevitably become a tendency for exporting renewable electricity to the local power grid. Such a feature will lead to an increased operating cost of a community energy system without building-vehicle energy interactions, whereas promising economic potentials are given to building-vehicle energy interactions for the enhancement in grid independence and renewable penetration. Contradiction between the increase of fuel cell degradation cost and the associated operating cost saving for the interactive building-vehicle energy system, has not been studied and addressed. In other words, if the fuel cell degradation is considered and the interactive building-vehicle network is still economically feasible, stakeholders will be highly motivated to deploy building-vehicle integration in practice. However, few studies give clear indications towards the impact of grid feed-in tariff on economic motivations of HVs' owners in interactive energy sharing networks with the consideration on fuel cell degradation.

This study aims to fill the abovementioned scientific gaps. To be more specific,

1) a two-space cabin thermal model is developed to calculate (1) the cabin indoor temperatures for passengers and PEMFCs; (2) energy consumption of vehicle HVAC systems under the effects of PEMFCs' heat release, outdoor climates, vehicle air changes, driving and parking schedules, and so on;
2) a fuel cell degradation model is proposed to quantify the decreased performance of vehicle PEMFCs caused by daily transportation and V2G interactions, based on a fuel cell stack voltage model in transportation [30]. The impact of V2G interactions on the fuel cell degradation is quantitatively and exclusively characterized;
3) a community-level electricity-H_2 hybrid energy network for the carbon-neutrality transition in California, U.S.A., is formulated, integrating low-rise single houses, rooftop PV systems, HVs, a H_2 station, local power grid, and local H_2 pipelines. The developed fuel cell degradation model and the two-space cabin thermal model are integrated in the energy network for techno-economic feasibility analysis;
4) in terms of the V2G interactions, trade-off strategies between the associated fuel cell degradation costs and the grid import cost savings are explored, through the parametrical analysis on HV quantity and grid feed-in electric tariff.

The analysis will show the importance of fuel cell degradation to avoid the techno-economic performance overestimation of regional energy systems. The paper structure is organized as follows: the research methodology is shown in Section 2. Results and discussion are in Section 3. Applications of research results and limitations are given in Section 4. Finally, the conclusion is presented in Section 5.

2 Methodology

2.1 Scenario, location, and climate

This study establishes a scenario of a residential community (20 single houses and 4 HVs with a nearby H_2 station), located in San Francisco (37 °N, 122 °W), California, U.S.A. California is a pioneer of clean energy application in the U.S.A., and it has established an ambitious target of increasing the renewable share ratio from current 30% to 60% of the total regional energy consumption by 2030 [40]. One of California's measures for actualizing the above target is to widely deploy H_2 energy infrastructures and commercial products with cleaner energy rather than fossil fuels in the transportation sector. Currently, California has built 42 H_2 stations for charging HVs [41], and plan to have at least one thousand H_2 stations and one million HVs by 2030, which can roughly achieve a reduction of around 2.63 million m^3 gasoline in the current transportation sector [42]. In the proposed community, the houses are connected to the local electric grid, and the H_2 station is connected to the local H_2 pipelines. The small quantity of HVs is for matching the current status that HVs and H_2 infrastructure are still under development [27].

San Francisco is characterized with cool climate and sufficient solar radiation. As shown in Fig. 1 (originally from our previous study [43]), the mean outdoor temperatures are 10-16 °C throughout the whole year, and the corresponding relative humidity is 70-80%. The local solar radiation is strong in summer (higher than 200 kWh/m^2 monthly from May to August), and it is relatively weak in winter (lower than 100 kWh/m^2 monthly from November to February). Similarly, the local wind speed is high in summer (higher than 5 m/s from May to August), and relatively low in winter (below 4 m/s from November to February).

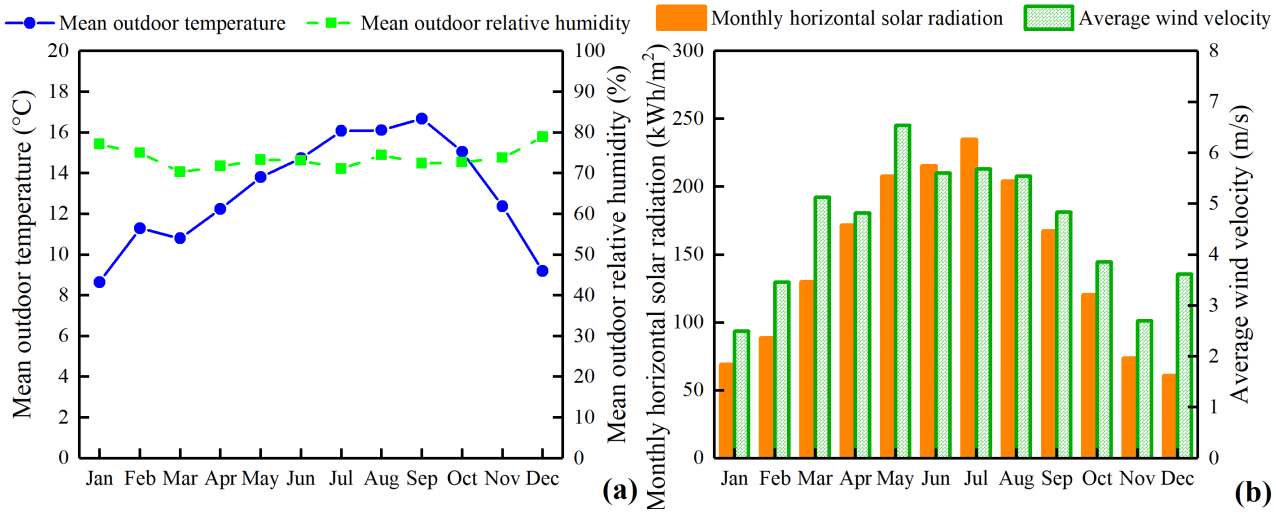

Fig. 1. Climate of San Francisco: (a) temperatures and humidity; (b) solar radiation and wind velocity (originally from our previous study [43]).

2.2 Buildings, renewable systems, local grid, and hydrogen station.

The detailed design and configuration of the buildings, renewable systems, local grid, and H_2 station have been presented in our previous study [43], and this section gives a concise description to show the key information.

2.2.1 Residential houses

The investigated buildings are single two-floor residential houses. Each floor is 200 m^2 with the internal heights at 3.0 m and 4.5 m for the ground and top floors, respectively. The houses adopt light-weight materials for walls, floors, ceilings, and roofs, and their thermal characteristics comply with the requirements of ASHRAE Standard 90.2 [44].

Each house has four occupants with 1.2-met metabolic rate (126 W) per person. The largest internal heat gains from the artificial lighting and electrical equipment indoors are 2 and 15 W/m^2, respectively. Due to the local cool climate,

the houses only have electrical space heating from November to February, with the indoor set-point temperatures at 20 °C for the ground floor (mainly living rooms and kitchens) and at 18 °C for the top floor (mainly bedrooms). The air change of the investigated houses is actualized by natural ventilation. The air change rates (ACR) are 0.5 h^{-1} when the outdoor environment is higher than 20 °C and 0.1 h^{-1} when it is below 20 °C. Moreover, in each house, the daily hot water consumption is 0.24 m^3 [45], with the supplying water temperature at 49 °C (120 °F) [46].

2.2.2 Rooftop photovoltaic systems

Each house is installed with 40-m^2 high-efficiency PV panels with the reference efficiency at 0.22 [47]. The corresponding temperature coefficient is -0.3%/°C. The tilted angle of PV panels is 45°, and the gap between the PV panels and the roof is 0.1 m. The detailed parameters of the rooftop photovoltaic systems will be shown in Section 2.7.

2.2.3 Local grid

Pacific Gas and Electric Company (i.e., PG&E) is one of major electric power providers in California. This study adopts its Time-of-Use Plan (E-Tou-D) [48] which uses different electric prices during different periods. To be specific, the peak period is 17:00-20:00 during weekdays, and the rest hours of the week belong to the off-peak period. Also, the electricity price is somewhat different between cool and warm seasons (as listed in Table 1). Meanwhile, PG&E has established a solar energy project to reduce house electricity cost, which is for promoting renewable energy application in California [49]. To be specific, the grid-imported electricity cost of a house can be compensated by exporting PV-generated electricity to the grid. Before the annual grid-imported electricity cost is fully compensated, the compensation price of PV-generated electricity is the same as that listed in Table 1. However, if a house with PV panels exports more electricity than the imported electricity from the grid within a year, the surplus grid-exported electricity will not be paid by the electric grid company. But the house owner who exports more electricity than the imported electricity can receive an additional reward from the local government. The reward quantity is dependent on the amount of annual net surplus electricity exported to the grid with the price at $0.03 per kWh [50].

Table 1. Cost information on the local grid.

Month	Electricity price ($/kWh)		Annual net surplus electricity reward ($/kWh)
	Peak period	Off-peak period	0.03
Jun-Sep	0.36540	0.27044	
Jan-May & Oct-Dec	0.29153	0.27415	

2.2.4 H_2 station

In the current situation, California's H_2 stations only supply H_2 to HVs for regional transportation, without any energy interactions with local buildings and other energy infrastructures. This study establishes multidirectional interactions between the H_2 station and its ambient buildings and vehicles to present the promising benefits of H_2-supported building-vehicle energy networks.

The investigated H_2 station is designed to have a daily dispensation of 100 kg H_2 for supporting local transportation. The H_2 station is connected to the local H_2 pipelines which supply H_2 gas, and the H_2 price for charging HVs is $16.51 per kg [51]. The integration of the community and the H_2 station is established by deploying a H_2 system in the H_2 station, which includes an electrolyzer with the maximum power of 150 kW for H_2 production and a compressor for compressing the produced H_2 to 700 bar. The surplus PV-generated electricity of the houses can be absorbed by the H_2 system to produce H_2 gas, which also helps release the grid burden through reducing the amount of grid-exported electricity. It should be noted that the H_2 system does not absorb any grid-imported electricity. Thus, the onsite-

produced H_2 is 100% renewable. After deploying the H_2 system, the H_2 station has two sources of H_2: (1) the electrolyzer in the H_2 station and (2) the local H_2 pipelines. For the electrolyzer, the idling power is 30 kW, which means that the input electric power for producing H_2 gas must be at least 30 kW. Moreover, the H_2 station is designed to store 500 kg onsite-renewable-produced H_2 at most.

Furthermore, a heat recovery system with a 6-m^3 water tank is deployed to recover heat from both the electrolyzer (when producing H_2 gas) and PEMFCs (during V2G interactions) for partly covering the hot water load of the houses. The detailed design of the heat recovery system is presented in our previous study [43] and the key parameters of the H_2 system are listed in Section 2.7.

2.3 Hydrogen-related parameters of vehicles

This study established a simplified HV model with the reference to a famous commercial product "Toyota Mirai 2016" [52], whose H_2 storage capacity, maximum storage pressure, maximum travel range, and maximum fuel cell power are 5 kg, 700 bar, 502 km, and 114 kW, respectively. In the investigated community, the HVs leave houses during the daytime (8:00-18:00) and park near houses at night (18:00-8:00) during weekdays. The HVs usually leave houses in the morning (9:00-12:00) during weekends. The daily travel distance (forth and back) is 50 km/vehicle with one hour (30 minutes for each trip, forth or back), and the H_2 consumption for transportation is 0.00996 kg/km.

Similar with our previous study [43], some assumptions are made to simplify the simulation work:

(1) The HVs are simplified as a combination of a storage system (i.e., a H_2 tank) and an energy consumption system (i.e., a PEMFC).

(2) HV tanks can be charged at the H_2 station (a) half an hour before HVs leave houses or (b) half an hour after HVs come back to houses.

(3) HV tanks are only discharged during transportation and V2G interaction processes. For transportation, due to the fast PEMFC power changes happening within seconds [30], the H_2 consumption of HVs is simply determined according to the actual distance and vehicle HVAC power (see Section 2.4). The output power of PEMFCs for transportation is simplified and determined according to the empirical model based on the H_2 consumption rate [53].

(4) For the PEMFCs, the idling power is 4.7 kW [54], which means that the lowest V2G power is 4.7 kW. If the building energy shortage power is lower than 4.7 kW, the PEMFCs will be inactive.

(5) The lowest fractional state of charge (SOC) of HV tanks must guarantee the tank safety (inner pressure must be at least 2 bar higher than the atmospheric pressure) and at least one-day transportation energy demand. Therefore, the lowest SOC of HV tanks (the lower SOC limit, i.e., $SOC_{lower,\ limit}$) is 0.11. When the $SOC_{lower,\ limit}$ is lower than 0.11, HVs will be charged to the SOC level at 0.95 (the upper SOC limit, i.e., $SOC_{upper,\ limit}$) at the H_2 station. Also, the V2G interaction only works when the SOC of HV tanks is higher than the $SOC_{lower,\ limit}$.

The detailed parameters of PEMFCSs are shown in Section 2.7.

2.4 Cabin thermal model

Cabin thermal environments have significant effects on the PEMFCs' performance. As described in Section 1.2, cabin thermal environments dominate the amount of vehicle PEMFCs' heat released to the ambient environment and the PEMFCs' cooling system. Besides, a comfortable cabin environment for drivers and passengers requires additional energy from vehicle PEMFCs for powering vehicle HVAC systems to regulate the cabin temperature. Therefore, it is needed to adopt a cabin thermal model for evaluating the real dynamic performance of PEMFCs.

A previous study on EVs developed a car-level lumped capacitance thermal network model for calculating cabin indoor temperatures and energy consumption of vehicle HVAC systems [55]. The original model is expressed as follows:

$$M_c \frac{dT_c}{dt} = K_{ac}(T_a - T_c) + K_{bc}(T_b - T_c) + q_{solar} + q_{hvac} \quad (1)$$

where M_c is the thermal mass of vehicle cabin (J/K); T_c is the cabin indoor temperature (°C); T_a is the outdoor air temperature (°C); T_b is the electrochemical battery temperature (°C), with the assumption that the electrochemical battery is attached to the passenger cabin; K_{ac} is the convective heat transfer coefficient between the outdoor air and vehicle cabin (W/K); K_{bc} is the heat transfer coefficient between the electrochemical battery and vehicle cabin (W/K); q_{solar} is the solar heat entering the cabin (W); q_{hvac} is the heat added or removed by the vehicle HVAC system (W); t is the time step (h).

With the reference to the mode for EVs [55], a two-space cabin thermal model of HVs is proposed for computational efficiency herein (Fig. 2), corresponding to the design of the referenced commercial product "Toyota Mirai 2016" [52]. The HV thermal model has two spaces (cabins): one is for the driver and passengers (Cabin 1), and another is for PEMFCs (Cabin 2, with a realistic assumption that the PEMFCs are not attached to Cabin 1). Therefore, for Cabins 1 or 2, the heat balance involves the heat transfer from the outdoor environment and the adjacent cabin.

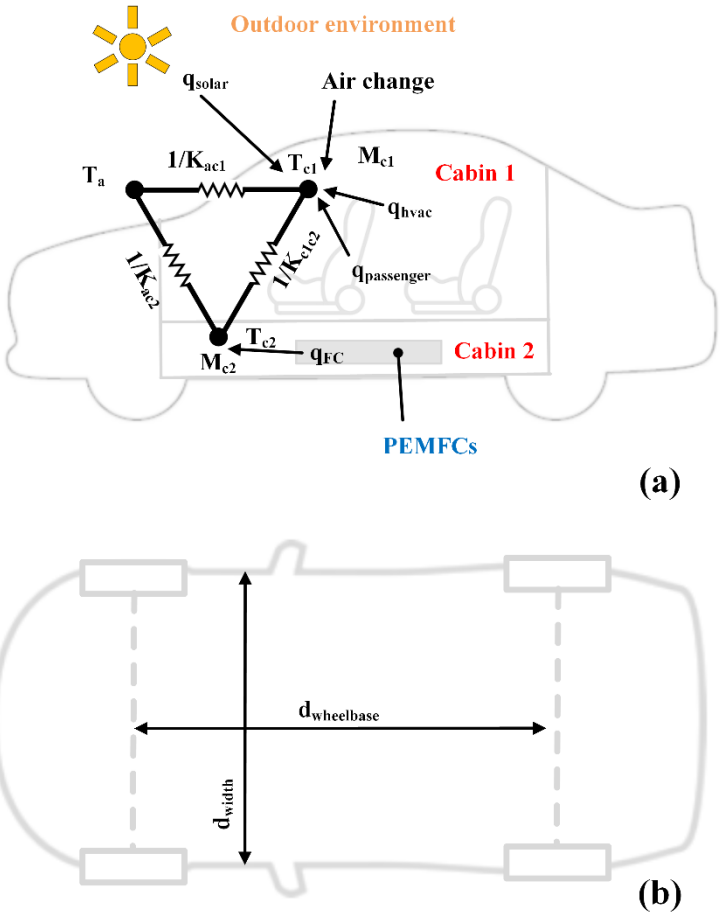

Fig. 2. The two-space cabin thermal model: (a) the lumped capacitance thermal network, and (b) the overhead view.

The two-space model includes the effects of vehicle ventilation with different air change rates during driving and parking processes. The two-space cabin thermal model for HVs is expressed as follows:

$$M_{c1} \frac{dT_{c1}}{dt} = K_{ac1}(T_a - T_{c1}) + K_{c1c2}(T_{c2} - T_{c1}) + n_{ach} m_{air,\,c1} c_{air}(T_a - T_{c1}) + q_{solar} + q_{passenger} + q_{hvac} \quad (2)$$

$$M_{c2} \frac{dT_{c2}}{dt} = K_{ac2}(T_a - T_{c2}) + K_{c1c2}(T_{c1} - T_{c2}) + q_{FC} \quad (3)$$

where M_{c1} is the thermal mass of Cabin 1 (J/K); M_{c2} is the thermal mass of Cabin 2 (J/K), which is assumed to be 30% of M_{c1}; T_{c1} is the indoor temperature of Cabin 1 (°C); T_{c2} is the indoor temperature of Cabin 2 (°C); K_{ac1} is the convective heat transfer coefficient between the outdoor air and Cabin 1 (W/K); K_{ac2} is the convective heat transfer coefficient between the outdoor air and Cabin 2 (W/K), which is assumed to be 30% of K_{ac1}; K_{c1c2} is the convective heat transfer coefficient between Cabin 1 and Cabin 2 (W/K); $q_{passenger}$ is the heat generated by the driver and passengers (W), and each person is 126 W; q_{FC} is the heat of PEMFCs entering Cabin 2 (W); n_{ach} is the air change rate of Cabin 1, which is 5 h^{-1} during driving and 1 h^{-1} during parking [56]; $m_{air,\,c1}$ is the air mass of Cabin 1 (kg), with the assumption that Cabin 1 has an inner space of 6 m^3 and the air density is 1.293 kg/ m^3; c_{air} is the air specific heat capacity (1003 J/ kg·K). Since the reference commercial product "Toyota Mirai 2016" has a very similar cabin size as that of "Toyota Prius" which was adopted in study [55], this study adopts the same or similar thermal values for the HV model. Moreover, it should be noted that this study adopts the different heat transfer coefficients between the cabin and outdoor air (K_{ac1} and K_{ac2}) during the driving and parking procedures. To be specific, according the estimation method of the study [57], the heat transfer coefficient between the cabin and outdoor air during the driving procedure (50 km/h) is about double that during the parking procedure. Therefore, this study adopts 22.6 W/K [55] and 45.2 W/K for K_{ac1} for the parking and driving modes, respectively. The detailed parameters are listed in Table 2.

In the mode above, one import factor affecting the cabin environment is solar heat gain (q_{solar}). The study [55] does not provide a detailed method of calculating vehicle's solar heat gain. With the reference to our previous study on indoor solar radiation in buildings [58], a simplified method is adopted to calculate vehicle solar heat gain. To be more specific, when calculating heat gain from solar radiation, the HV geometry is simplified as a horizontal plate which has a size of the cabin's projected area on the horizontal ground (see Fig. 2(b)), with the assumption that the HV size is negligible when comparing with the sky and sun. The solar heat has two approaches entering the cabin: one is through the semi-transparent windows, and the other is through heat conduction by the heated cabin envelope (including vehicle rooftops, windows, doors, and other surfaces). The total solar heat transfer coefficient will be decided by the characteristics of cabin envelope. The assumption above significantly reduces the computational complexity with the complicated vehicle driving and parking conditions with various locations and directions. The method of calculating vehicle solar heat gain is proposed as follows:

$$q_{solar} = I_{horizontal} \times \alpha_{overall} \times f_{eff} \times d_{wheelbase} \times d_{width} \tag{4}$$

where $I_{horizontal}$ is the total solar radiation intensity at the horizontal plate outdoors (W/m^2); $\alpha_{overall}$ is the overall solar heat absorptivity of Cabin 1; f_{eff} is the effective surface fraction of Cabin 1 directly exposed to strong solar radiation, which is 0.7 herein (for example, when the sunshine is from the left side of Cabin 1, the right side of Cabin 1 receives much less solar radiation, and thus the effective cabin surface exposed to strong solar radiation is reduced); $d_{wheelbase}$ is the wheelbase of the HV, which is almost the same as the length of Cabin 1 (2.78 m); d_{width} is the width of Cabin 1 (1.82 m). Moreover, $\alpha_{overall}$ is calculated as follows:

$$\alpha_{overall} = f_{window}\left(\tau_{window} + 0.5\alpha_{window}\right) + 0.5 f_{shell}\alpha_{shell} \tag{5}$$

where f_{window} is the surface fraction of Cabin 1 windows, which is the ratio of the window surface area to the total surface area of Cabin 1, and it is 0.4 herein; f_{shell} is the surface fraction of Cabin 1 shell (the non-transparent envelope), which is the ratio of the shell surface area to the total surface area of Cabin 1, and it is 0.6 herein; τ_{window} is the transmittance of Cabin 1 windows (0.4 [59]); α_{window} is the absorptivity of Cabin 1 windows (0.4 [59]); α_{shell} is the absorptivity of Cabin 1 shell (0.26 [59]); 0.5 represents that 50% of the solar heat absorbed by the windows or shell enters the cabin indoor environment, while the rest is dissipated into the outdoor environment (the solar-heated windows and shell have two-direction heat transfer: one towards the cabin indoor environment, and the other towards

the outdoor environment).

Besides, the coefficient of performance (COP) of the vehicle HVAC system is set at 2.5 [55]. The maximum cooling power of the vehicle HVAC systems is 4500 W, and the maximum heating power is 4000 W [55]. Another assumption is that the vehicle HVAC system can directly use the heat from the PEMFCs' cooling system for heating Cabin 1, and the maximum heat recovery power is 3000 W. Namely, when it is needed to heat the Cabin 1, only when the heating load is higher than 3000 W, the HVAC system will start and consume extra electricity from PEMFCs. Thus, the actual maximum heating power (vehicle HVAC system + heat recovery from the PEMFCs) is 7500 W herein.

Moreover, the cabin cooling set-point is set at 26 °C, and the heating set-point is 20 °C. To be specific, during the driving process (key-on), when temperature in the Cabin 1 is higher than 26 °C or lower than 20 °C in the previous time step, the vehicle HVAC system will be turned on. The HVAC load ($q_{hvac,\ load}$) is calculated as follows:

$$q_{hvac,\ load} = K_{ac1}(T_a - T_{c1}) + K_{c1c2}(T_{c2} - T_{c1}) + n_{ach} m_{air,\ c1} c_{air}(T_a - T_{c1}) + q_{solar} + q_{passenger} \quad (6)$$

A positive value of $q_{hvac,\ load}$ means that the Cabin 1 needs cooling, and a negative value means that Cabin 1 needs heating.

When the HVAC is on and the load does not exceed the maximum heating or cooling capacity, it is assumed that the indoor temperature of the Cabin 1 is maintained at the set-point, and the heat balance of the Cabin 1 is expressed as follows:

When cooling:

$$0 = K_{ac1}(T_a - 26) + K_{c1c2}(T_{c2} - 26) + n_{ach} m_{air,\ c1} c_{air}(T_a - 26) + q_{solar} + q_{passenger} + q_{hvac} \quad (7)$$

When heating:

$$0 = K_{ac1}(T_a - 20) + K_{c1c2}(T_{c2} - 20) + n_{ach} m_{air,\ c1} c_{air}(T_a - 20) + q_{solar} + q_{passenger} + q_{hvac} \quad (8)$$

When the HVAC is on but the load exceeds the maximum heating or cooling capacity, the heat balance of the Cabin 1 is expressed as follows:

When cooling:

$$M_{c1}\frac{dT_{c1}}{dt} = K_{ac1}(T_a - T_{c1}) + K_{c1c2}(T_{c2} - T_{c1}) + n_{ach} m_{air,\ c1} c_{air}(T_a - T_{c1}) + q_{solar} + q_{passenger} - 4500 \quad (9)$$

When heating:

$$M_{c1}\frac{dT_{c1}}{dt} = K_{ac1}(T_a - T_{c1}) + K_{c1c2}(T_{c2} - T_{c1}) + n_{ach} m_{air,\ c1} c_{air}(T_a - T_{c1}) + q_{solar} + q_{passenger} + 7000 \quad (10)$$

Table 2. Key parameters of the two-space cabin thermal model.

Parameter	Description	Value
M_{c1}	Thermal mass of Cabin 1	101771 J/K
M_{c2}	Thermal mass of Cabin 2	0.3×M_{c1} J/K
T_a	Outdoor air temperature	Situation dependent, °C
T_{c1}	Indoor temperature of Cabin 1	Situation dependent, °C
T_{c2}	Indoor temperature of Cabin 2	Situation dependent, °C
K_{ac1}	Convective heat transfer coefficient between outdoor air and Cabin 1	45.2 W/K during driving
		22.6 W/K during parking

K_{ac2}	Convective heat transfer coefficient between outdoor air and Cabin 2	0.3×45.2 W/K during driving 0.3×22.6 W/K during parking
K_{c1c2}	Convective heat transfer coefficient between Cabin 1 and Cabin 2	3.468 W/K
$q_{passenger}$	Heat generated by the driver and passengers	126 W/person
q_{FC}	Heat of PEMFCs entering Cabin 2	Situation dependent
n_{ach}	Air change rate of Cabin 1	5 h^{-1} during driving 1 h^{-1} during parking
$m_{air,\ c1}$	Air mass of Cabin 1	7.758 kg
c_{air}	Air specific heat capacity	1003 J/kg·K
q_{hvac}	Heat added or removed by the vehicle HVAC system	Max 4500W for cooling Max 4000W for heating
$I_{horizontal}$	Total solar radiation intensity at the horizontal plate outdoors (W/m^2)	Situation dependent, W/m^2
f_{eff}	Effective surface fraction of Cabin 1 exposed to strong solar radiation	0.7
$d_{wheelbase}$	Wheelbase of the HV	2.78 m
d_{width}	Width of Cabin 1	1.82 m
f_{window}	Surface fraction of Cabin 1 windows	0.4
f_{shell}	Surface fraction of Cabin 1 shell	0.6
τ_{window}	Transmittance of Cabin 1 windows	0.4
α_{window}	Absorptivity of Cabin 1 windows	0.4
α_{shell}	Absorptivity of Cabin 1 shell	0.26

5. *Fuel cell degradation model*

As described in Section 1.2, the fuel cell voltage drop brings two main effects: (1) the decreased maximum output power [30], and (2) the decreased energy conversion efficiency which means the decreased output power with the same H_2 consumption rate of fuel cells [37]. This study adopts the stack voltage degradation model [30] for evaluating the fuel cell degradation due to transportation, and revises it to evaluate the degradation caused by both daily transportation and V2G interactions. In the original model [30], during the transportation process, the fuel cell degradation is caused by large load changing cycles, start-stop cycles, idling time, and maximum power time. The fuel cell degradation rate by transportation ($r_{d,\ HVtran}$, %/h) is calculated as follows:

$$r_{d,\ HVtran} = k_p \times \left(P_1 n_1 + P_2 n_2 + P_3 t_1 + P_4 t_2\right) \tag{11}$$

where k_p is the accelerating coefficient at 1.72 [30]; P_1 (%/circle), P_2 (%/circle), P_3 (%/h), and P_4 (%/h) are the performance deteriorate rates caused by the large-range load change cycling, start-stop cycling, idling condition, and maximum power condition, respectively. n_1, n_2, t_1, and t_2 are the load changing cycle frequency (circle/h), start-stop cycle frequency (circle/h), idling time fraction per hour, and maximum power load time fraction per hour. According to the study [30], P_1 (%/circle), P_2 (%/circle), P_3 (%/h), and P_4 (%/h) are 0.00005893%/circle, 0.00196%/cycle,

0.00126%/h, and 0.00147%/h, respectively; n_1, n_2, t_1, and t_2 are 56 cycles/h, 0.99 cycles/h, 13/60, and 14/60, respectively. It should be noted that the start-stop circle frequency in the study [30] was calculated using the data of the tests with each trip lasting for hours. In this study, the actual start-stop cycle quantity is calculated according to the trip quantity. Namely, a daily forth-back travel has two trips (forth and back trips and each one has a start-stop cycle) and the total time of two trips is one hour. Thus, n_2 is 2 cycles/h herein.

The fuel cell degradation by transportation ($D_{FC,\ HVtran}$, %) is calculated as follows:

$$D_{FC,\ HVtran} = \int_0^{t_{end}} r_{d,\ HVtran}(t)dt \tag{12}$$

where t_{end} is the end time of the simulation.

An important assumption of the original model [30] is that during transportation, the PEMFCs' power is at the idling power or the maximum power, or switches between these two powers. In the original model, within one hour of driving, a HV can have 56 times of large load changing cycles, but less than 30 minutes of idling and maximum powers. However, for V2G interactions, PEMFCs are usually assumed to have relatively stable output powers within seconds or minutes, and the power can be in the middle between the idling and maximum powers. Therefore, during the V2G process, it is assumed that the fuel cell degradation rate is caused by large load changing cycles, start-stop cycles, and actual PEMFC powers. The fuel cell degradation rate by V2G interactions ($r_{d,\ V2G}$, %/h) is calculated as follows:

$$r_{d,\ V2G} = k_p \times \left(P_1 n_1 + P_2 n_2 + P_5\right) \tag{13}$$

where P_5 is the performance deteriorate rate caused by the actual output power (%/h). A simplified interpolation method is adopted to calculate P_5 as follows:

$$P_5 = P_3 + \left(P_4 - P_3\right) \times \left(P_{FC,\ actual} - P_{idling}\right) / \left(P_{FC,\ max} - P_{idling}\right) \tag{14}$$

where $P_{FC,\ max}$ is the original maximum PEMFC power without any degradation (kW); $P_{FC,\ actual}$ is the actual PEMFC power (kW); $P_{FC,\ idling}$ is the PEMFC idling power (kW).

The fuel cell degradation by V2G interactions ($D_{FC,\ HVtran}$, %) is calculated as follows:

$$D_{FC,\ V2G} = \int_0^{t_{end}} r_{d,\ V2G}(t)dt \tag{15}$$

For a HV, the total fuel cell degradation (D_{FC}) is the sum of the degradation caused by transportation and V2G interactions. Thus, the total fuel cell degradation is calculated as follows:

$$D_{FC} = D_{FC,\ HVtran} + D_{FC,\ V2G} \tag{16}$$

As described above, the fuel cell degradation will lead to the decrease in the maximum power and energy efficiency of fuel cells. The actual maximum PEMFC power ($P_{FC,\ max,\ actual}$) of a HV is calculated as follows:

$$P_{FC,\ max,\ actual} = D_{FC} \times P_{FC,\ max} \tag{17}$$

Similarly, the actual PEMFC power ($P_{FC,\ actual}$) under a certain H_2 consumption rate or PEMFC current is calculated as follows:

$$P_{FC,\ actual} = D_{FC} \times P_{FC,\ designed} \tag{18}$$

where $P_{FC,\ designed}$ is the designed PEMFC output power under a certain H_2 consumption rate or PEMFC current without any degradation.

2.6 The interactive building-vehicle energy network and energy management strategies

As shown in Fig. 3, the proposed building-vehicle energy network integrates the houses, HVs, H_2 station, local power grid, and local H_2 pipelines (the network framework is originally from our previous study [43]). The vehicle cabin

model and fuel cell degradation model are established by the Python programming language (Python 3.8), and the rest components of the building-vehicle network are established by the energy simulation software, TRNSYS 18 [60].

In the proposed network, the renewable energy is generated by the PV systems installed on the house rooftops, to partly cover building and transportation energy demands. The surplus renewable is exported to the community micro-grid (B2G interaction) which connects to the local power grid and the nearby H_2 station. When the surplus renewable electricity in the micro-grid is exported to the H_2 station through the micro grid (G2S interaction) and is absorbed by the H_2 system (the electrolyzer and compressor), it is used to produce H_2 gas which is then stored in the H_2 station. The H_2 station is also connected to the local H_2 pipelines. Therefore, charging HV tanks at the H_2 station (S2V interaction) may utilize two H_2 sources: one is from the onsite-renewable-generated H_2, and the other one is from the local-pipe-delivered H_2. Vehicle PEMFCs can discharge the H_2 in HV tanks to power vehicle engines for transportation or the micro-grid (V2G interaction) for covering energy demand shortage. Moreover, the connection of the community micro-grid to the local power grid will absorb surplus renewable energy and cover building demand shortage, which finally balances the power in micro-grid. Furthermore, to increase the H_2 energy efficiency, a heat recovery system is designed to collect the warm water produced by the electrolyzer and PEMFCs during the G2S and V2G processes. The warm water in a water tank is to partly cover the heating load of domestic hot water. To ensure the safety of PEMFCs, a special two-stage heat recovery system is designed to realize the non-mixed heat recovery, and the detailed design is presented in our previous study [43]. Through configuring such a building-vehicle energy network, the community can achieve high energy flexibility, grid power stability, and significant energy cost saving [43].

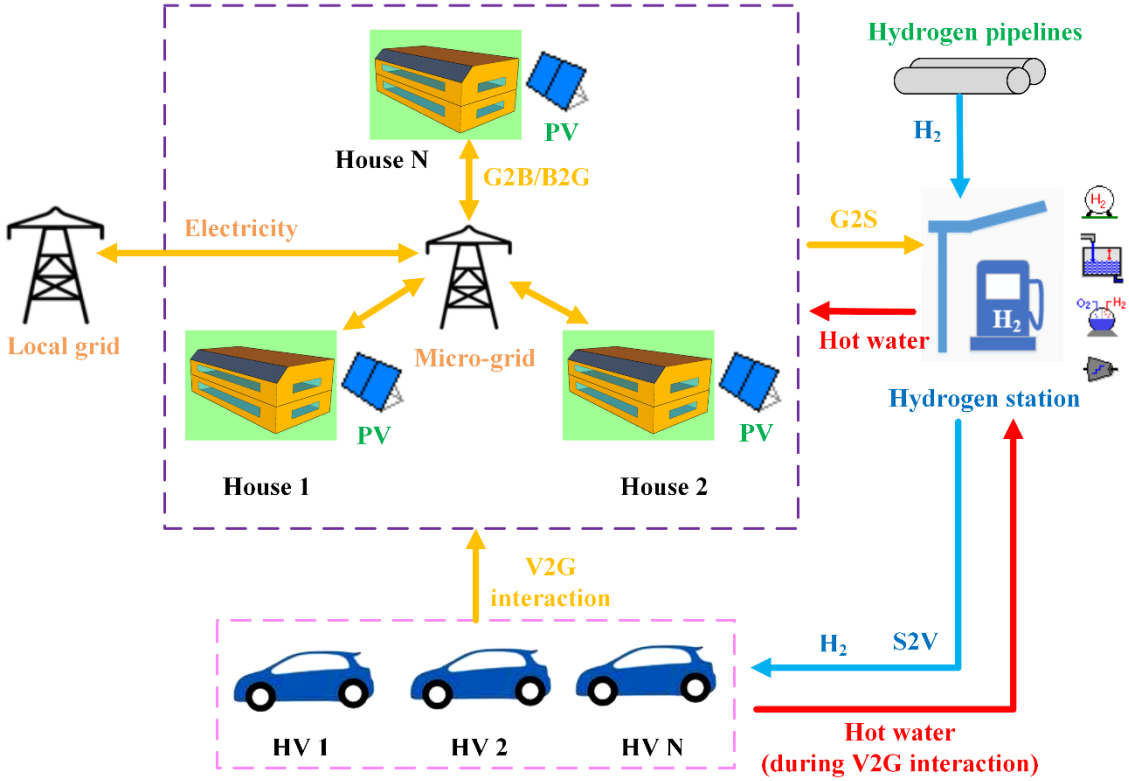

Fig. 3. The structural configuration of the H_2-based district energy community integrating single houses, rooftop PV powered, fuel-cell-powered HVs, a H_2 station, local H_2 pipelines, community micro-grid, and local power grid.
(G2B means the grid-to-building interaction; B2G means the building-to-grid interaction; G2S means the grid-to-H_2-station interaction; S2V means the H_2-station-to-vehicle interaction; V2G means the vehicle-to-grid interaction.)

The main goal of this study is to quantify the fuel cell degradation and to highlight the importance to avoid the techno-economic performance overestimation in building-vehicle energy networks. To actualize this goal, three cases

are proposed, including (1) a reference case without neither V2G interactions nor fuel cell degradation, and (2) two formal cases integrating V2G interactions for enhancing energy flexibility: i.e., one formal case with the fuel cell degradation and the other one without fuel cell degradation. Through the comparative analysis among the three cases, the effects of fuel cell degradation on energy flexibility and cost of the building-vehicle networks can be determined.

The detailed control logics of the three cases are described below:

(1) Reference case (Fig. 4(a)): The community formulates an energy-sharing micro-grid which connects all houses, rooftop PV panels, and local power grid. The micro-grid is also connected to the nearby H_2 station, and thus the renewable electricity of the community can be converted to H_2 gas through the H_2 system in the H_2 station. The micro-grid is designed with the function that the surplus renewables partly cover transportation energy demands. To be specific, the HVs will be charged at the H_2 station with the H_2 produced by the onsite renewables and also the H_2 delivered by the local H_2 pipelines. Such an energy system configuration also reduces the renewable congestion of the local grid since much renewable electricity is consumed by the H_2 system rather than being exported to the local grid. In this case, no V2G interactions are deployed, and the fuel cell degradation is not considered.

For the whole network, the renewable energy (P_{REe}) is used to firstly cover the building energy demand (L_e) (Fig. 4(b)):

a) If P_{REe} is higher than L_e, the excessive renewable ($P_{REe,\,surp1} = P_{REe} - L_e$) is exported to the local grid.

b) If P_{REe} is below L_e, the energy demand shortage ($P_{short1} = L_e - P_{REe}$) is covered by the electricity imported from the local grid.

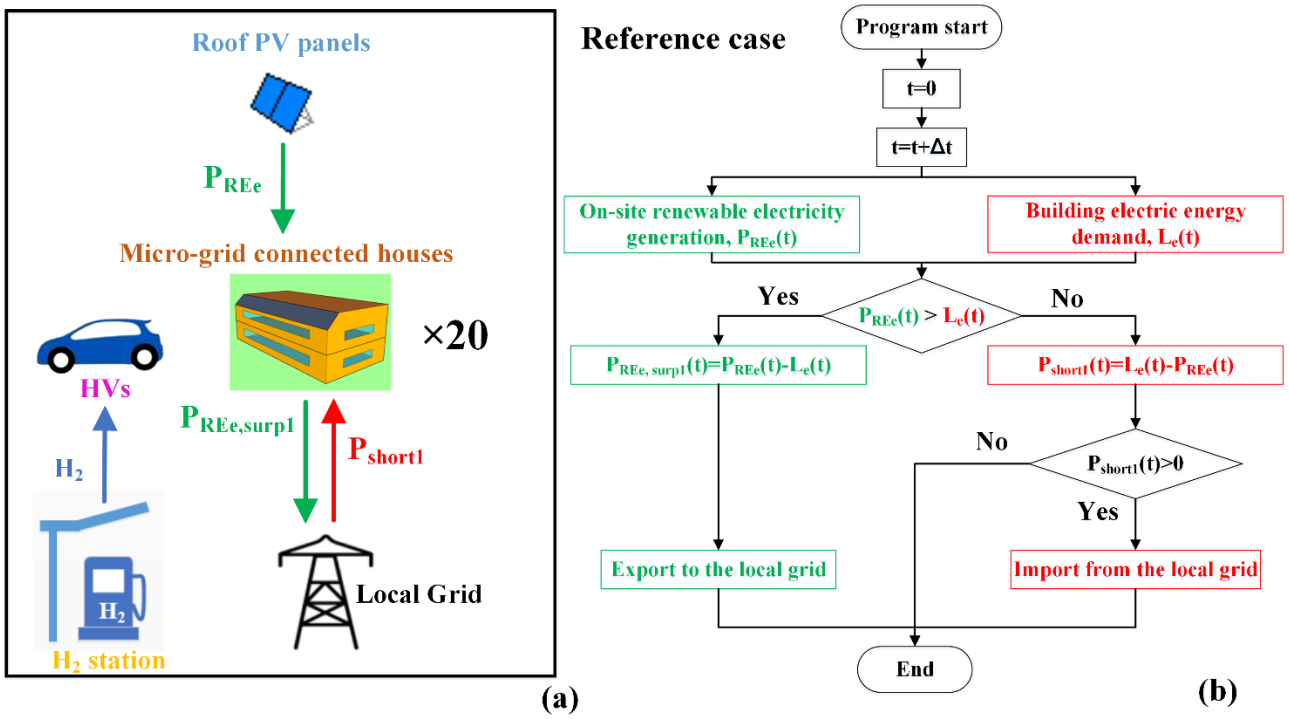

Fig. 4. (a) Energy flow pathway and (b) rule-based control strategy of the reference case (originally from [43]).

(2) Case 1 (Fig. 5(a)): The community energy network configuration is almost the same as that of the reference case. The only difference is that V2G interactions are deployed for covering building energy shortage. To be specific, when the accumulated onsite-renewable-generated H_2 is higher than the accumulated H_2 consumption for covering daily transportation, ($H2_{RE,\,store} > 0$), the H_2 in vehicle tanks can be discharged to power the community micro-grid during the demand shortage period. Such a feature contributes to the enhancement in the energy independence and the burden

reduction in the local power grid. Moreover, in this case, the fuel cell degradation is still not considered, corresponding to the common assumption of relevant existing studies. In other words, the maximum V2G power of a HV is constant and stable at 114 kW.

Again, in the energy network, the renewable energy (P_{REe}) is used to firstly cover the building energy demand (L_e) (Fig. 5(b)):

a) If P_{REe} is higher than L_e, the magnitude of the surplus renewable ($P_{REe,\ surp1} = P_{REe} - L_e$) decides whether it is exported to the local grid or absorbed by the H_2 system at the H_2 station. To be specific, if $P_{REe,\ surp1}$ is below the sum of the idling power ($P_{ely,\ idling}$) of the electrolyzer and the compressor power (P_{comp}), it will be directly released into the local grid, since it is unable to activate the electrolyzer for H_2 production. If $P_{REe,\ surp1}$ is beyond the sum of the idling power ($P_{ely,\ idling}$) of the electrolyzer and the compressor power (P_{comp}), and meanwhile the stored onsite-renewable-generated H_2 mass ($H2_{RE,\ store}$) at the H_2 station did not reach the storage limit of the onsite-renewable-generated H_2 ($H2_{RE,\ store,\ limit}$ = 500 kg) in the previous dynamic state, the $P_{REe,\ surp1}$ will be delivered to the H_2 system for producing H_2 gas. If $P_{REe,\ surp1}$ is beyond the sum of the idling power ($P_{ely,\ idling}$) of the electrolyzer and the compressor power (P_{comp}), and meanwhile in the previous dynamic state, $H2_{RE,\ store}$ increased to $H2_{RE,\ store,\ limit}$, $P_{REe,\ surp1}$ will be exported to the local power grid. Furthermore, if the $P_{REe,\ surp1}$ exceeds the sum of the powers of the electrolyzer (P_{ely}) and the compressor (P_{comp}), the excessive renewable ($P_{REe,\ surp2}$) is exported to the local grid.

b) If P_{REe} is lower than L_e, the demand shortage ($P_{short1} = L_e - P_{REe}$) can be covered by the output power of vehicle PEMFCs ($P_{H2,\ dischar}$) but only in the condition that $H2_{RE,\ store}$ is beyond zero, the fractional state of charge of HV tanks (SOC_{HV}) higher than $SOC_{lower,\ limit}$, and P_{short1} higher than the PEMFCs' idling power ($P_{FC,\ idling}$) at the same time. Otherwise, P_{short1} is covered by the local grid. Besides, if P_{short1} exceeds the available $P_{H2,\ dischar}$, the unfilled demand shortage ($P_{short2} = P_{short1} - P_{H2,\ dischar}$) is covered by the electricity imported from the local grid.

(3) Case 2 (Fig. 5(a)): The community energy network configuration and the control logic are almost similar to that of Case 1. The only difference is that the fuel cell degradation is considered in both vehicle transportation and V2G interactions. To be specific, as described in Section 2.5, besides the decreased energy conversion efficiency, the maximum V2G power of a HV will decrease, along with the increase in accumulated fuel cell degradation . The actual maximum output power of a HV is calculated according to the magnitude of fuel cell degradation (see Section 2.5). Meanwhile, the fuel cell degradation cost is added in the operating cost of the whole community, which is described in Section 2.8.

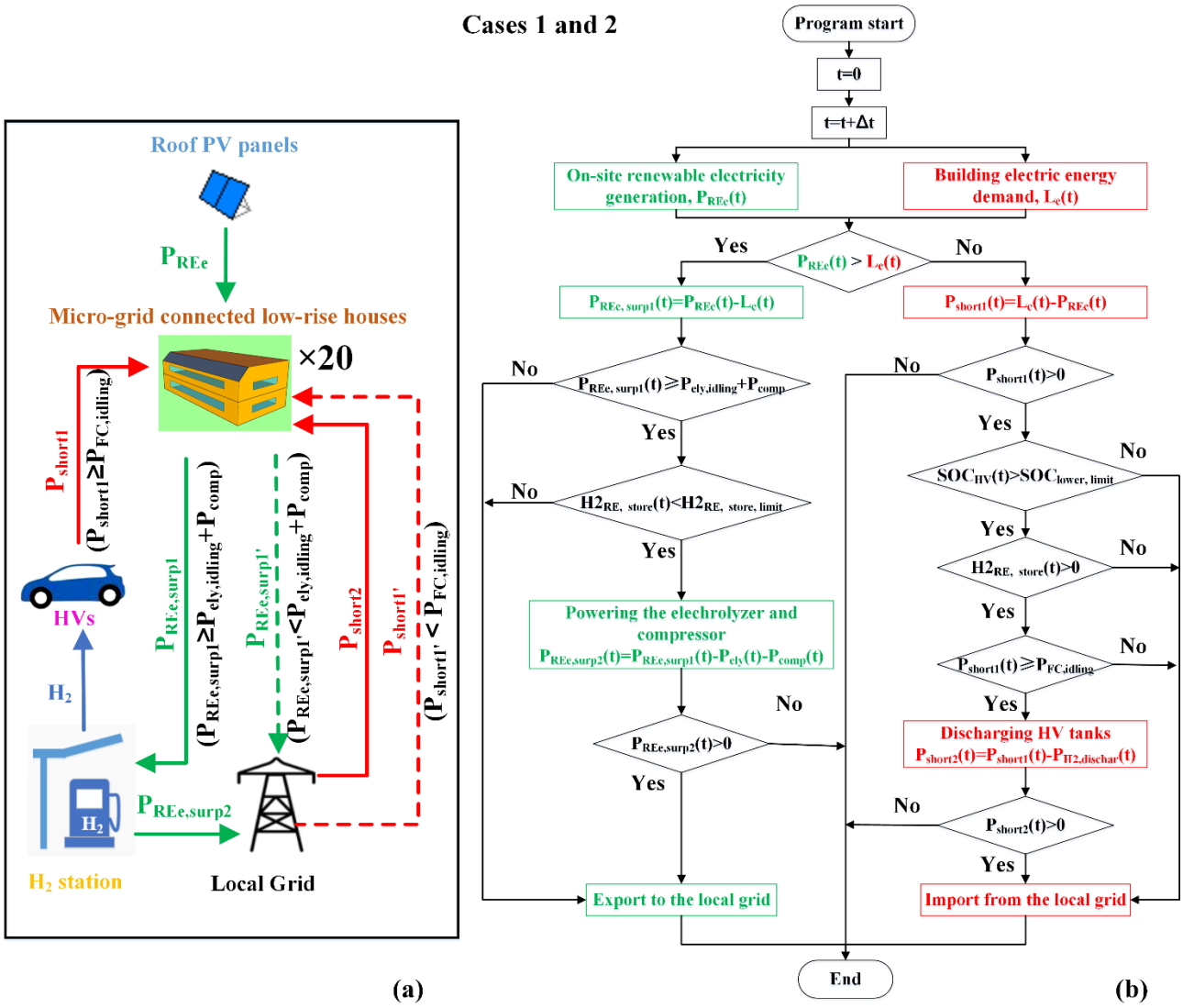

Fig. 5. (a) Energy flow pathway and (b) rule-based control strategy of Cases 1 and 2 (originally from [43]).

2.7 Key parameters of the building-vehicle energy network

This study couples the software of TRNSYS 18 [60] and Python 3.8 for the dynamic simulations of fuel cell degradation and energy flexibility. The time step of the simulation is set at 0.25 h. The key parameters of model components are listed in Table 3.

Table 3. Key parameters of the building-vehicle energy network in TRNSYS.

Component	Parameter	Value
PV panels	Type in TRNSYS 18	567
	Collector length (m)	20
	Collector width (m)	2
	Channel height (m)	0.1
	Reference PV efficiency	0.22 [47]
	Temperature coefficient (/°C)	-0.003

Electrolyzer	Type in TRNSYS 18	160a
	Electrode area (m^2)	0.5
	Number of cells per stack	20
	Number of stacks	2
	Cooling water inlet temperature (°C)	20
	Cooling water flow rate (m^3/h)	0.6
	Operating temperature (°C)	80
Compressor	Type in TRNSYS 18	167
	Number of parallel compressors	1
	Number of compressor stages	3
	Desired pressure (bar)	700
HV hydrogen tank (for 4 HVs)	Type in TRNSYS 18	164b
	Maximum pressure (bar)	700
	Tank volume (m^3)	0.488
PEMFC	Type in TRNSYS 18	170a
	Number of cells per stack	60
	Number of stacks	6
	Electrode area (cm^2)	1000
	Coolant inlet temperature (°C)	30
	Coolant temperature rise (°C)	30
H_2 station	Type in TRNSYS 18	Self-developed
	Daily dispensing H_2 (kg/day)	100
	Maximum stored onsite-renewable-produced H_2 (kg)	500
Domestic tankless heater	Type in TRNSYS 18	138
	Maximum heating rate (kW)	80
	Set-point temperature (°C)	49
Heat exchanger (for two-stage cooling)	Type in TRNSYS 18	5
	Load side inlet temperature (°C)	20
	Overall heat transfer coefficient (W/K)	2000
Water tank	Type in TRNSYS 18	39
	Overall tank volume (m^3)	6
	Tank circumference (m)	10
	Cross-sectional area (m^2)	6
	Wetted loss coefficient ($kJ/h \cdot m^2 \cdot K$)	1.5

Wetted loss coefficient (kJ/h·m²·K)		1.0

2.8 Assessment criteria

2.8.1 Grid interaction

For actualizing the energy balance of the community micro-grid, the local power grid absorbs the surplus renewable electricity and covers the building demand shortage. The magnitudes of grid interactions are evaluated by the grid-imported power (P_{imp}) and the grid-exported power (P_{exp}). The low grid-imported and grid-exported powers mean the low grid burden and high flexibility of the community. In order to distinguish the grid status, P_{imp} is represented by positive values and P_{exp} is represented by negative values.

2.8.2 Fuel cell degradation

As described in Section 2.5, for each HV, the annual total fuel cell degradation is the sum of (1) the degradation by daily transportation ($D_{FC,\ HVtran}$) and (2) the degradation by V2G interactions ($D_{FC,\ V2G}$). For the latter degradation, the calculation is simplified and assumed that each HV "averagely" participates in V2G interactions. Namely, all the HVs share the total fuel cell degradation caused by V2G interactions ($D_{FC,\ V2G,\ total}$). For each HV, the total fuel cell degradation (D_{FC}) is calculated as follows:

$$D_{FC} = D_{FC,\ HVtran} + D_{FC,\ V2G,\ total} / n_{HV} \tag{19}$$

2.8.3 Energy operating cost

The total operating cost of the investigated community includes the costs of electricity, H_2, and fuel cell degradation.

Based on Table 1, within one year, the grid-imported electricity cost (IC, \$/a) and the grid-exported electricity compensation (EC, \$/a) are calculated below:

$$IC_{peak,\ mon,\ i} = E_{imp,\ peak,\ mon,\ i} \times R_{peak,\ mon,\ i} \tag{20}$$

$$IC_{off\text{-}peak,\ mon,\ i} = E_{imp,\ off\text{-}peak,\ mon,\ i} \times R_{off\text{-}peak,\ mon,\ i} \tag{21}$$

$$IC = \sum_{i=1}^{12} (IC_{peak,\ mon,\ i} + IC_{off\text{-}peak,\ mon,\ i}) \tag{22}$$

$$EC_{peak,\ mon,\ i} = E_{exp,\ peak,\ mon,\ i} \times R_{peak,\ mon,\ i} \tag{23}$$

$$EC_{off\text{-}peak,\ mon,\ i} = E_{exp,\ off\text{-}peak,\ mon,\ i} \times R_{off\text{-}peak,\ mon,\ i} \tag{24}$$

$$EC = \sum_{i=1}^{12} (EC_{peak,\ mon,\ i} + EC_{off\text{-}peak,\ mon,\ i}) \tag{25}$$

where $E_{import,\ peak,\ mon,\ i}$ and $E_{import,\ off\text{-}peak,\ mon,\ i}$ are the amounts of grid-imported electricity during the peak period and the off-peak period of the i-th month, respectively (kWh/month); $R_{peak,\ mon,\ i}$ and $R_{off\text{-}peak,\ mon,\ i}$ are the electricity prices during the peak period and the off-peak period of the i-th month, respectively (\$/kWh); $IC_{peak,mon,i}$ and $IC_{off\text{-}peak,mon,i}$ are the costs of the amounts of grid-imported electricity during the peak period and the off-peak period of the i-th month, respectively (\$/month); $E_{export,\ peak,\ mon,\ i}$ and $E_{export,\ off\text{-}peak,\ mon,\ i}$ are the amounts of grid-exported electricity during the peak period and the off-peak period of the i-th month, respectively (kWh/month); $EC_{peak,mon,i}$ and $EC_{off\text{-}peak,mon,i}$ are the economic compensations by the grid-exported electricity amounts during the peak period and the off-peak period of the i-th month, respectively (\$/month).

Within one year, the electricity cost ($C_{e,\ 1}$, \$/a) is the net cost between the grid-imported cost and grid-exported compensation, as calculated by Equation (26):

$$C_{e,1}=\begin{cases} IC-EC & \text{if } IC > EC \\ 0 & \text{if } IC \le EC \end{cases} \quad (26)$$

The annual net grid-electricity consumption of the community is calculated as follows:

$$E_{net,annual}=\int_0^{t_{end}} P_{imp}(t)dt-\int_0^{t_{end}} P_{exp}(t)dt \quad (27)$$

where $E_{net,\ annual}$ is the annual net electricity consumption (kWh/a).

The additional reward due to the annual net renewable electricity exportation ($C_{e,\ 2}$, \$/a) is calculated as follows:

$$C_{e,2}=\begin{cases} \left(-E_{net,\ annual}\right)\times 0.03 & \text{if } E_{net,\ annual} < 0 \\ 0 & \text{if } E_{net,\ annual} \ge 0 \end{cases} \quad (28)$$

Therefore, the total annual electricity cost (C_e, \$/a) is calculated as follows:

$$C_e = C_{e,1}-C_{e,2} \quad (29)$$

For the investigated community, the annual net H_2 consumption ($H_{net,\ annual}$, kg/a) includes the H_2 used for daily transportation and for V2G interactions, and it is calculated as follows:

$$H_{consume,\ annual}=\int_0^{t_{end}} [M_{HVtran,\ H2}(t)+M_{V2G,\ H2}(t)]dt \quad (30)$$

$$H_{produce,\ annual}=\int_0^{t_{end}} M_{RE,\ H2,\ building}(t)dt \quad (31)$$

$$H_{net,\ annual}=H_{consume,\ annual}-H_{produce,\ annual} \quad (32)$$

where $H_{consume,\ annual}$ is the annual consumed H_2 by the community (kg/a); $H_{produce,\ annual}$ is the annual produced H_2 using renewable electricity from the building-integrated rooftop PV systems (kg/a); $H_{net,\ annual}$ is the annual net H_2 consumption (kg/a); $M_{HVtran,\ H2}(t)$ is the H_2 consumed by vehicle PEMFCs for covering transportation demands at the t-th time step (kg/h); $M_{V2G,\ H2}(t)$ is the H_2 consumed by vehicle PEMFCs for V2G interaction at the t-th time step (kg/h); $M_{RE,\ H2,building}(t)$ is the H_2 produced using the renewable electricity of the rooftop PV systems at the t-th time step (kg/h). If $H_{net,\ annual}$ is less than zero, it indicates that the whole community produces more H_2 than it consumes.

In 2020, the H_2 cost in California is 16.51 \$/kg [51]. Since California has not established any policies for the compensation price of onsite-renewable-generated H_2, the annual cost of H_2 (C_{H2}, \$/a) is simply calculated according to the annual net H_2 consumption of HVs:

$$C_{H2}=H_{net,\ annual}\times 16.51 \quad (33)$$

The PEMFCs' price is \$11000 for each vehicle [38]. The degradation threshold is assumed to be 20% (namely, when the accumulated degradation is 20%, the fuel cell should be replaced), and the fuel cell degradation cost is \$550/% (assuming the equivalent fuel cell degradation cost within the degradation threshold). The annual cost of fuel cell degradation (C_{FC}, \$/a) is calculated according to the annual fuel cell degradation of each vehicle (D_{FC}):

$$C_{FC}=D_{FC}\times n_{HV}\times 550 \quad (34)$$

The total annual energy operating cost (C_{energy}, \$/a) is calculated below:

$$C_{energy}=C_e+C_{H2}+C_{FC} \quad (35)$$

3 Results and discussion

3.1 Comparative analysis among the cases with and without fuel cell degradation

3.1.1 Energy response and grid interaction of the community

Within one year, the PV-generated electricity and the energy demand are 12271.5 kWh and 8748.4 kWh per household, respectively. Besides, the annual transportation energy demand is 183.1 kg H_2 per vehicle (not considering fuel cell degradation and vehicle HVAC energy), with the total travel distance reaching 18250 km per vehicle.

Fig. 6 illustrates the dynamic energy response and grid power in the three cases. The values are mean hourly power, i.e., the mean value of powers at a certain time point of a day. For the local grid, the positive values mean the grid-import powers (the community imports electricity from the local grid), and the negative values mean grid-export powers (the community's renewable electricity is exported to the local grid). In the reference case, due to the isolation between the community and H_2 station, the local power grid suffers from heavy burdens of renewable congestion and demand shortage. To be specific, during the daytime, the grid-export power reaches up to 99.2 kW during the non-heating period (March to October) and 68.1 kW during the heating period (November to February). While during the nighttime, the grid-import power reaches up to 76.0 kW during the non-heating period and 94.4 kW during the heating period. In Cases 1 and 2, the renewable congestion and demand shortage are much ameliorated with and the integration of the community and H_2 station and the V2G interactions. To be specific, in Case 1, the grid-export powers are up to 20.0 and 8.4 kW during the non-heating and heating periods, respectively. Meanwhile, the grid-import powers are up to 22.2 and 46.1 kW during the non-heating and heating periods, respectively. In Case 2, the grid-export powers are up to 20.0 and 8.4 kW during the non-heating and heating periods, respectively. Meanwhile, the grid-import powers are up to 22.3 and 45.4 kW during the non-heating and heating periods, respectively. As compared to the reference case, in Cases 1 and 2, deploying V2G interactions reduces the grid-export and grid-import powers by more than 80% and 50%, respectively. The reason of more stable grid powers in Cases 1 and 2 can be attributed to the H_2 energy storage. To be specific, in Cases 1 and 2, 183163.2 and 183147.9 kWh renewable electricity, which is about 75% of the annual renewable electricity, are absorbed by the electrolyzer and compressor at the H_2 station, producing 3468.8 and 3468.5 kg H_2, respectively. However, in the reference case, the surplus renewable electricity is exported to the local grid. Meanwhile, in Cases 1 and 2, V2G interactions consume 2574.9 and 2601.8 kg onsite-renewable-generated H_2 to provide 40751.4 and 41056.3 kWh electricity for the community, respectively, covering about 28% of the community's annual energy demand. However, in the reference case, the building demand shortage is fully covered by the local grid. Furthermore, according to the comparison between Cases 1 and 2, the fuel cell degradation does not significantly change the grid stability, which can be attributed to the limited fuel cell degradation in the short term (see Section 3.1.2).

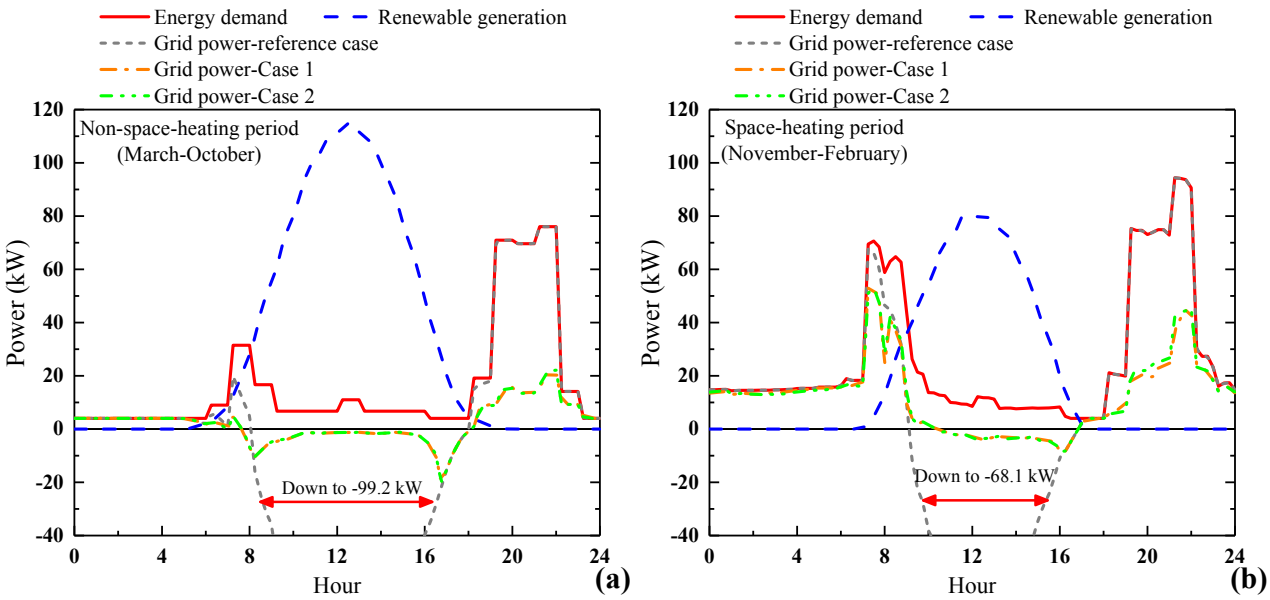

Fig. 6. Grid power of the building-vehicle energy network: (a) non-space-heating period and (b) space-heating period.

3.1.2 Cabin thermal environments and fuel cell degradation

Fig. 7 illustrates the cabin mean hourly indoor temperatures in the three cases. The main finding is that V2G interactions will increase cabin indoor temperatures during the nighttime. In the reference case without V2G interactions, due to the strong solar radiation, the air temperature in Cabin 1 (for drivers and passengers) reaches up to 40-50 and 25-28 °C at noon (11 a.m. to 2 p.m.) during the non-space-heating and space-heating periods, respectively. The air temperature in Cabin 2 (for PEMFCs) is about 40 °C at 8-9 a.m. and 6-7 p.m. due to the transportation. When V2G interactions are deployed in the community (Cases 1 and 2), Cabin 1 still shows the peak indoor temperature up 40-50 and 25-28 °C at noon (11 a.m. to 2 p.m.) during the non-space-heating and space-heating periods, respectively. Meanwhile, the air temperature in Cabin 2 (for PEMFCs) is about 40 °C at 8-9 a.m. and 6-7 p.m. due to the transportation. Nonetheless, due to V2G interactions at night when vehicle PEMFCs release a lot of heat to the cabin space, in Cases 1 and 2, during 8-11 p.m., the air temperature in Cabin 2 can be up to 7 °C higher than that in the reference case without V2G interactions. The reason is that the V2G interactions will increase the operating state on fuel cells, and lead to the associated heat released to the Cabin. Moreover, it should be noted that the sudden temperature increase of Cabin 2 is due to PEMFCs' intermittent running for transportation. The sudden temperature drop of Cabin 1 at around 12 p.m. (Fig. 7(a)) is due to the running of vehicle HVAC system during the transportation on weekends.

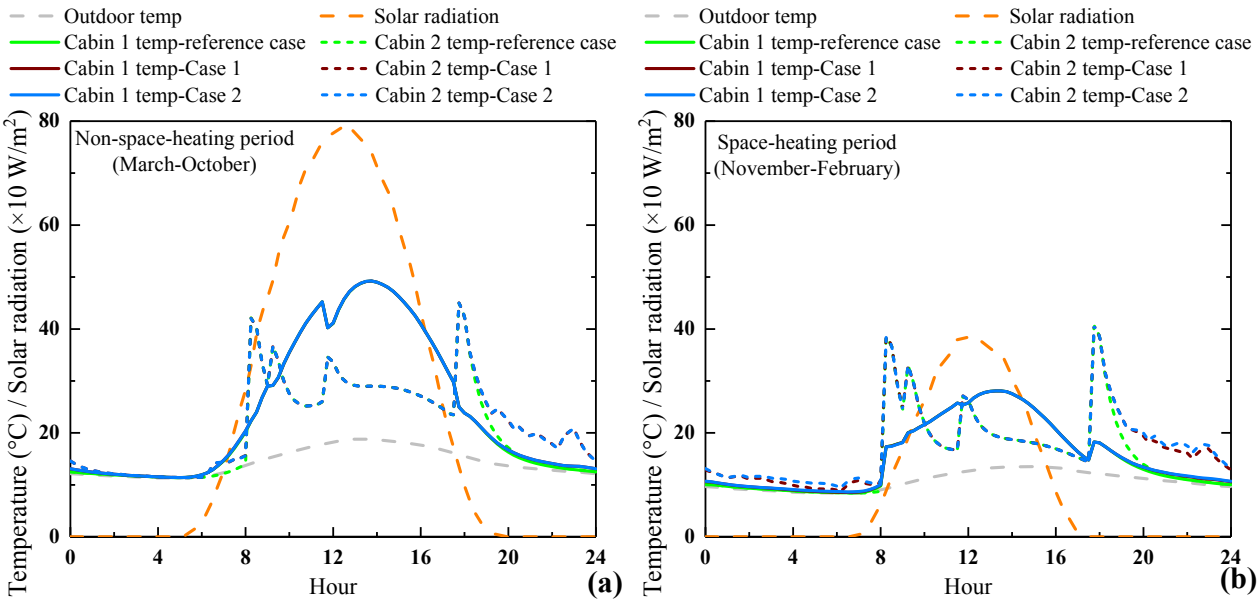

Fig. 7. Cabin indoor temperatures: (a) non-space-heating period and (b) space-heating period.

Fig. 8 shows the annual fuel cell degradation in the Case 2. Obviously, in the proposed building-vehicle energy network, daily transportation is the main source of the fuel cell degradation. Specifically, within one year, the fuel cell degradation caused by the daily transportation is 2.50% per vehicle, consisting of 2.0848%, 0.0294%, 0.1714%, and 0.2153% by the large-range load change cycling, start-stop cycling, idling condition, and maximum power condition, respectively. Meanwhile, the fuel degradation caused by V2G interactions is 0.66% per vehicle, consisting of 0.0021%, 0.0055%, and 0.6484% by the large-range load change cycling, start-stop cycling, and actual output power, respectively. Totally, the fuel cell degradation is 3.16% per vehicle within one year, of which 79.1% and 20.9% are caused by daily transportation and V2G interactions, respectively. Since this study adopts the fuel cell replace threshold at 20%, if the HVs are only for transportation, the vehicle PEMFCs need to be replaced every 8 years. If the HVs are for both daily transportation and V2G interactions, the vehicle PEMFCs need to be replaced every 6.3 years. Namely, the V2G interaction increases the fuel cell degradation speed by 26.4% as compared to the condition when vehicle PEMFCs are only for transportation. Therefore, although V2G interactions achieve high grid flexibility of the community (see Section 3.1.1), the significant effects of fuel cell degradation with shortened service lifetime on the energy performance of the building-vehicle network should not be ignored.

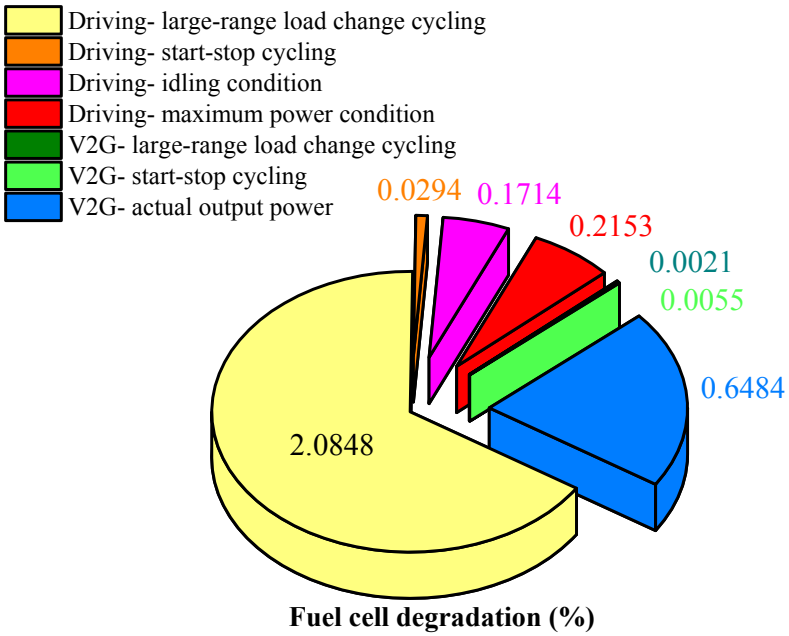

Fig. 8. Fuel cell degradation distribution.

3.1.3 Annual energy operating cost

Fig. 9 illustrates the annual operating costs of the community in the cases with and without considering fuel cell degradation. The most important finding is that the fuel cell degradation accounts for a consideration proportion in the total energy operating cost of the community. To be specific, in the reference case without V2G interactions, due to the high-level compensation of renewable electricity [49], the grid-imported electricity cost can be fully compensated, and the grid cost is below zero (-$1745.7), meaning that the house owners can receive the payment from the local government for exporting renewable electricity to the local grid. Besides, the H_2 cost is $12274.5 in the reference case, since the H_2 for daily transportation is entirely imported from the local pipelines. Such a result also indicates that the transportation energy cost could be far beyond the building energy cost in regional building-vehicle-isolated energy networks. In Case 1 with V2G interactions but without considering fuel cell degradation, since about 75% of the renewable electricity is used for H_2 production rather than being exported to the local grid for compensating the grid cost (see Section 3.1.1), the annual grid cost reaches up to $15562.2, much higher than that in the reference case. However, the H_2 cost is significantly reduced to -$2484.4, meaning that at the end of the year, part of renewable H_2 is still stored in the H_2 station. Therefore, the total operating cost in Case 1 is $13077.7. In Case 2 with V2G interactions and fuel cell degradation, the grid cost and H_2 cost are $15675.6 and -$1850.1, respectively, slightly higher than those of Case 1. Besides, in Case 2, the total fuel cell degradation cost of the building-vehicle energy network is $6945.2, reaching 33.4% of the total operating cost ($20770.61). As compared to Case 2, if fuel cell degradation is not considered (Case 1), the energy operating cost of the building-vehicle energy network will be underestimated by about 37%, revealing that the cost by fuel cell degradation should not be ignored in practice.

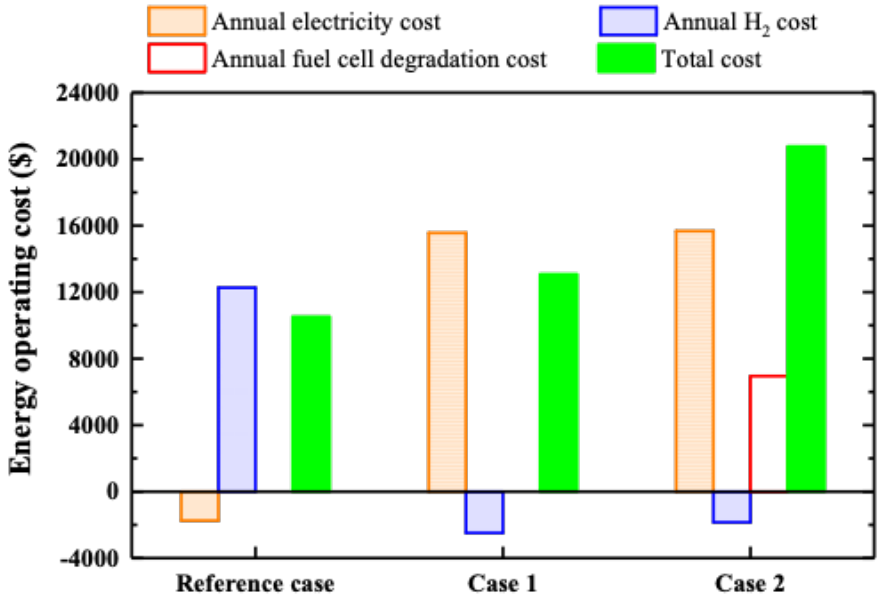

Fig. 9. Cost comparison between the cases with and without considering fuel cell degradation.

Furthermore, according to the results presented in Fig. 6, 7, and 9, the building-vehicle energy network will motivate the grid operator to include the HVs as an additional high-stability energy storage for reducing the grid burden, since fuel cell degradation will not cause significant changes in V2G interactions. Meanwhile, since fuel cell degradation will not significantly change the cabin indoor environment, the HV users, who are also the residential building owners, will be highly motivated if the economic benefits of the reduced grid import cost is higher than the degradation cost of fuel cells.

3.2 Effects of fuel cell degradation on grid interaction and energy operating cost with the increased fuel-cell-driven vehicle quantity

Due to the promising blue print in the near future [27], HVs are going to be more popular than now. Namely, in a local community, the quantity of HVs is expected to increase in the coming years. The increased HVs might lead to two main effects on the investigated community:

(1) The higher burden on the local power grid, since more onsite-renewable-generated H_2 is used for daily transportation and less onsite-renewable-generated H_2 is for V2G interactions to cover building energy shortage;

(2) The increased energy operating cost due to the increased consumption of pipe-delivered H_2 for daily transportation and the increase in accumulated fuel cell degradation of HVs.

To demonstrate the effects of fuel cell degradation with the increased HV quality, the HV quantity is set at four to twenty with an increasing step of two, corresponding to the assumption that 20%-100% of the single houses in the community (totally 20 households) have HVs. The comparison between Cases 1 and 2 with the increased HV quantity reveals the importance of fuel cell degradation in building-vehicle energy networks.

Fig. 10 illustrates the mean hourly grid power with the increased HV quantity. In the reference case, since there are no connections among the HVs, buildings, and H_2 station, the grid power does not change with the increased HV quantity as the HVs are completely supported by the pipeline delivered hydrogen (thus only one line is drawn for the reference case). The most significant finding is that the increased HV quantity will increase the grid burden, and the fuel cell degradation will not cause obvious changes in the grid power in the short term if the HV quantity is constant. To be specific, in Case 1 where the fuel cell degradation is not considered, when the HV quantity increases from four to twenty, the maximum grid-import power increases from 22.2 to 74.4 kW and from 46.1 to 93.7 kW during the non-

space-heating and the space-heating periods, respectively. The grid-export power does not change much because most of the annual renewable electricity has already been exported to the H_2 system at the H_2 station (see Section 3.1.1) when there are four HVs, and increasing the HV quantity does not significantly increase the amount of renewable electricity for the H_2 system. In Case 2 where the fuel cell degradation is considered, when the HV quantity increases from four to twenty, the maximum grid-import power increases from 22.3 to 74.9 kW and from 45.4 to 93.8 kW during the non-space-heating and the space-heating periods, respectively. The comparison between Cases 1 and 2 with the same HV quantity indicates that, the grid interactions are almost the same, which can be attributed to the slight fuel cell degradation in the short term (this point will be explained in the following paragraph).

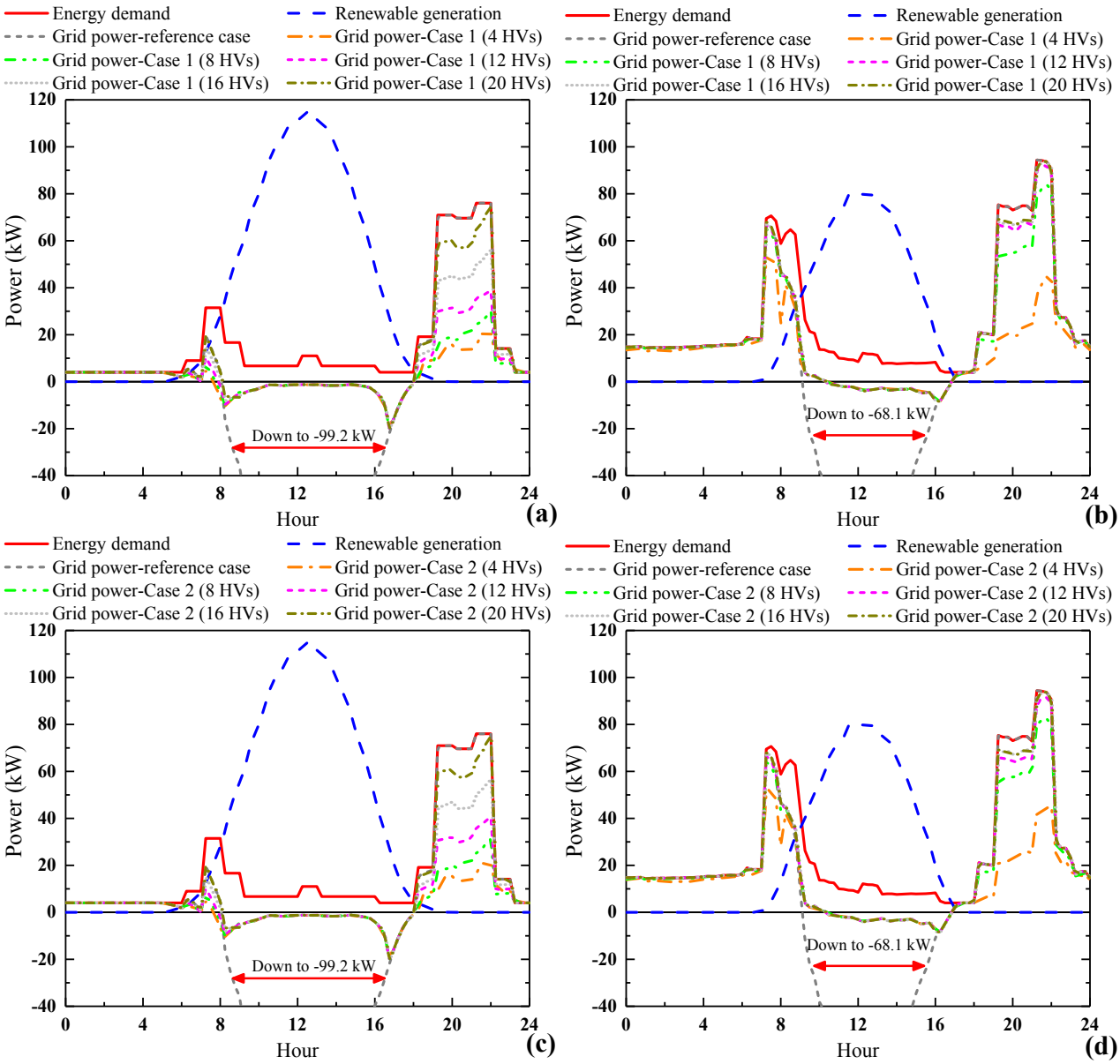

Fig. 10. The grid power with the increased HV quantity in Case 1 during (a) non-space-heating period and (b) space-heating period, and in Case 2 during (c) non-space-heating period and (d) space-heating period.

As shown in Fig. 11, the increased HV quantity of the community reduces each HV's fuel cell degradation by V2G interactions. To be specific, within one year, the fuel cell degradation of each HV is 3.16% when the HV quantity is four (see Section 3.1.2). When the HV quantity increases from four to twenty, the fuel cell degradation of each HV slightly decreases to 2.50%. Such a small degradation in the fuel cell efficiency will not cause obvious changes in V2G

interactions in the short term, such as one year. Moreover, considering that the fuel cell degradation by daily transportation is 2.5% (as described in Section 3.1.2), the fuel cell degradation by V2G interactions decreases from 0.66% to 0 when the HV quantity increases from four to twenty. The decreased degradation by V2G interactions for each HV can be attributed to two reasons: (1) the reduced V2G energy interaction due to the reduced H_2 amount for V2G interactions, and (2) the less shared V2G degradation due to the increased HV quantity. For example, when the community has four HVs, totally 2601.8 kg onsite-renewable-generated H_2 is used for V2G interactions and the total fuel cell degradation by V2G interactions is 2.62%, with the fuel cell degradation by V2G interactions at 0.66% for each HV. When the community has twelve HVs, totally 1230.6 kg onsite-renewable-generated H_2 is used for V2G interactions and the total fuel cell degradation is 1.20%, with the fuel cell degradation by V2G interactions at almost 0.1% for each HV.

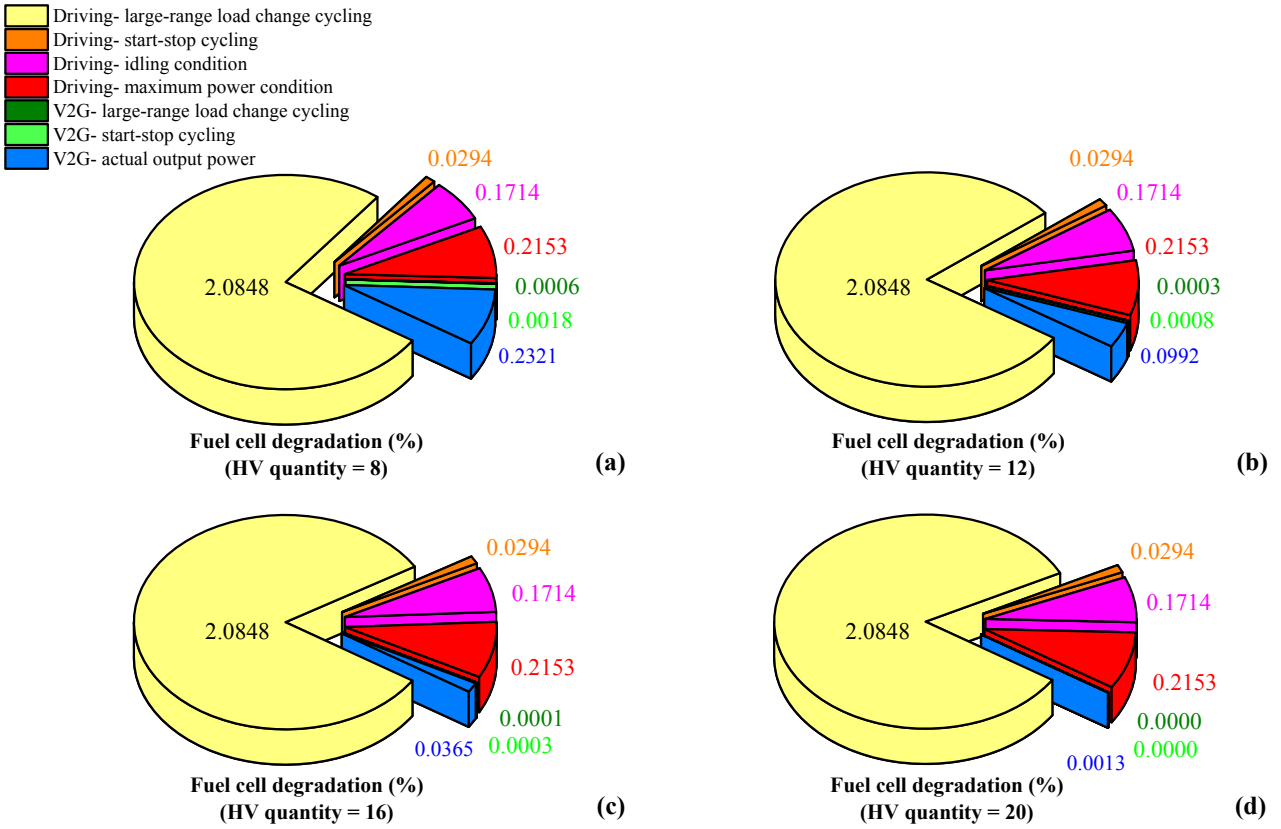

Fig. 11. The fuel cell degradation distribution of the building-vehicle energy network with the HV quantities at (a) eight, (b) twelve, (c) sixteen, and (d) twenty.

Fig. 12 shows how the energy operating cost changes with the increased HV quantity. It is clear that elevating the HV quantity in the community significantly increases the energy operating cost, and the fuel cell degradation cost. In the reference case, when the HV quantity increases from four to twenty, the grid cost keeps stable at -$1745.7 and the H_2 cost increases from $12274.5 to $60106.3, resulting in the increase of total operating cost from $10528.7 to $58360.6. In Case 1 where the fuel cell degradation is not considered, when the HV quantity increases from four to twenty, the grid cost and H_2 cost increase from $15562.2 to $32291.6 and from -$2484.4 to $3891.0, respectively, resulting in the increase of total operating cost from $13077.7 to $36182.6. In Case 2 with fuel cell degradation, when the HV quantity increases from four to twenty, the grid cost, H_2 cost, and fuel cell degradation cost increase from $15675.6 to $32438.9, from -$1850.1 to $4315.1, and from $6945.2 to $27524.6, respectively. Correspondingly, the total operating cost increases from $20770.6 to $64278.6, by over 200%. Meanwhile, in Case 2, the ratio of the fuel cell degradation cost to

the total operating cost increases from 33.4% to 42.8%. Moreover, as compared to Case 2, if the fuel cell degradation is not considered (Case 1), as the HV quantity increases from four to twenty, the energy operating cost will be underestimated by 37%-44%. Such a finding indicates that, as the HV quantity increases, the fuel cell degradation will become the main sector in the energy operating cost of regional energy systems.

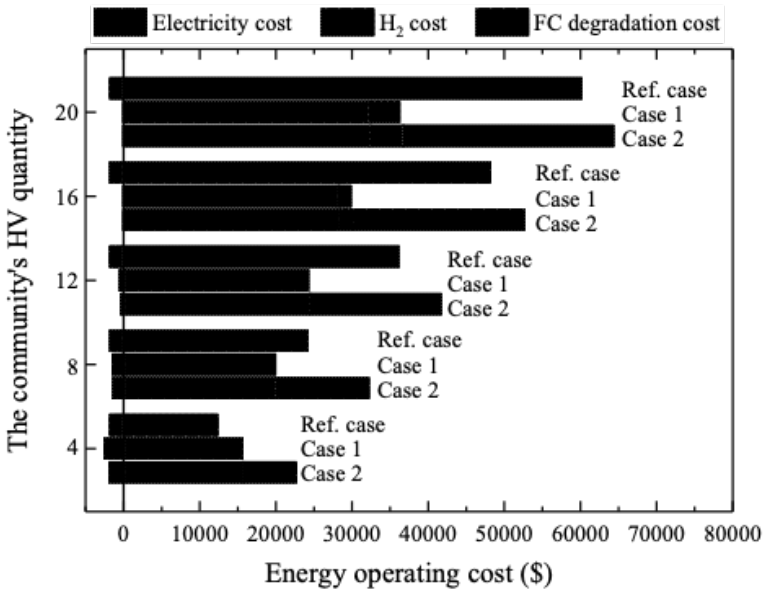

Fig. 12. The energy operating cost of the building-vehicle network with the increased HV quantity.

3.3 Effects of fuel cell degradation on energy operating cost with the decreased renewable electricity price

Under the current grid feed-in tariff with high-price renewable electricity in California [49], compared to the isolated buildings and vehicles system, the building-vehicle-integrated community is not economically competitive, as the renewable energy being exported to the grid will bring more economic benefits than the renewable energy being shared to vehicles with fuel cell degradation. In the near future, the renewable electricity price will probably decline, along with the continuous increase in renewable electricity production [39]. Namely, although California still has a high price for the renewable electricity for promoting the regional carbon-neutralization strategy now, the high-price-renewable era probably ends up in the coming years, falling to the low-price-renewable status as what happened in Europe [39].

The decreased renewable electricity price will result in two main effects on the interactive building-vehicle energy sharing community:

(1) Instead of being exported to the power grid, the onsite surplus renewable can be shared in vehicles, so as to reduce the grid import cost during the demand shortage period. The interactive building-vehicle energy sharing community might become more economically competitive than the system without V2G interactions;

(2) The reduced proportion of the fuel cell degradation cost to the total operating cost. To be specific, in a certain community, the decreased renewable electricity price or the increased grid electricity cost due to the elevated grid electricity price will increase the total energy operating cost. As a result, the unchanged fuel cell degradation cost will account for a reduced proportion to the total energy operating cost.

The vehicle integration in district buildings in Cases 1 and 2 can reduce the grid cost, since the electricity-H_2-electricity procedure will store the low-price renewable electricity and cover the building demand shortage, so as to reduce the high-price grid-imported electricity. The decreased energy operating cost with V2G interactions might achieve a higher cost efficiency than that without V2G interactions. Moreover, if the renewable electricity price is very low or even zero, the cost saving by V2G interactions might even compensate the fuel cell degradation cost. If so, the

proposed building-vehicle energy network will become more economically competitive in practice.

To demonstrate the effects of fuel cell degradation with the decreased renewable electricity price, this section lowers the renewable electricity price from the 100% original price (same as that of the grid-imported electricity, as shown in Table 1) to 0 with a decreasing step of 20%. Other parameters are still kept the same as those described in Section 2 (20 houses and 4 HVs). The comparison among the reference case and Cases 1 and 2 will indicate the economic competitiveness and effectiveness of V2G interactions, and the importance of fuel cell degradation in the near future with decreased economic incentives of renewable energy. The assessment criterion is the energy operating cost since the non-economic performances of the three cases will remain unchanged as only the renewable electricity price is changed.

Fig. 13 shows the impact of renewable electricity price on the energy operating cost. Obviously, the decreased renewable electricity price improves the economic competitiveness of the building-vehicle energy network with V2G interactions. To be specific, in the reference case without deploying V2G interactions or considering fuel cell degradation, when the decreasing magnitude of renewable electricity price increases from 0 to 100%, the H_2 cost keeps stable at -$1850.1, but the grid cost increases from -$1745.7 to $37302.9, resulting in the increase of the total operating cost from $10528.7 to $49577.4. In Case 1 where V2G interactions are deployed but the fuel cell degradation is not considered, when the decreasing magnitude of renewable electricity price increases from 0 to 100%, the grid cost increases from $15562.2 to $19727.0, resulting in the increase of total operating cost from $13077.7 to $17242.6. The energy operating cost of Case 1 is lower than that of the reference case when the decreasing magnitude of renewable electricity price is 40% or higher. In Case 2 with fuel cell degradation, when the decreasing magnitude of renewable electricity price increases from 0 to 100%, the grid cost increases from $15675.6 to $19843.5, resulting in the increase of the total operating cost from $20770.6 to $24938.5. Correspondingly, the proportion of fuel cell degradation cost to the total operating cost decreases from 33.4% to 27.8%. The energy operating cost of Case 2 is lower than that of the reference case when the decreasing magnitude of renewable electricity price is 60% or higher. Such a finding indicates that the fuel cell degradation cost accounts for a large amount share in the building-vehicle network with the decreased renewable price. Moreover, it should be noted that the fuel cell degradation cost by daily transportation is $5502.0 (2.5%/3.16%×$6945.2, see Sections 3.1.2 and 3.1.3). If the reference case also considers the fuel cell degradation (only caused by transportation), the energy operating cost of Case 2 is lower than that of the reference case when the renewable electricity price is reduced by 40% or more. Namely, the cost saving by deploying V2G interactions can compensate the fuel cell degradation cost when the renewable electricity price of California is reduced by more than 40%.

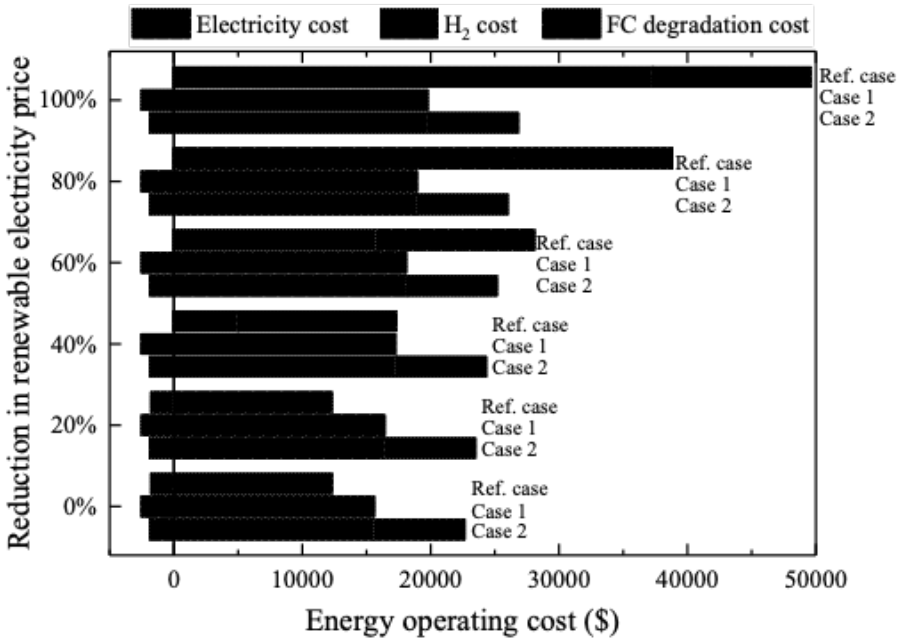

Fig. 13. The energy operating cost of the building-vehicle network with the decreased renewable electricity price.

4 Applications and limitations

Integrating H_2 energy infrastructure, buildings, and local power grid is a promising approach to promote regional carbon neutralization with high energy flexibility, reduced grid burden, and low energy cost. However, the dynamic working thermal environment and degradation of vehicle PEMFCs are usually ignored in existing relevant studies. This study establishes a two-space cabin thermal model and a fuel cell degradation model to calculate the ambient temperature, energy output, efficiency, and operating cost of vehicle PEMFCs. To quantify the effects of fuel cell degradation, these two models are integrated with a community-level building-vehicle energy network consisting of PV systems, single houses, HVs, a H_2 station, local power grid, and local H_2 pipelines. The grid interaction and energy operating cost of the network are also explored with the increased HV quantity and the decreased renewable electricity price, which are the foreseeable trend in the near future. This study provides potential promising applications as follows:

(1) The cabin thermal model and the fuel cell degradation model proposed in this study provide a practical and fast approach and tool to calculate the detailed working environment, energy output performance, and operating energy cost of PEMFCs in the building-vehicle energy network, under the influences of the local climate. These two models will make the energy network more realistic than the existing relevant studies where the cabin heat transfer and fuel cell degradation are usually ignored. The enormous fuel cell degradation cost highlights the necessity to be considered, so as to avoid the performance overestimation in building-vehicle networks. Moreover, these models and their corresponding findings can also be applied or referenced in other regions with different types of buildings, as long as researchers, engineers, or designers adopt different input values according to their own projects.

(2) Currently, the H_2 infrastructure in California is under development, and the predesigned function for supporting local transportation only might limit its further application and development. This study indicates that integrating the H_2 infrastructure and HVs with the local buildings has a large potential of reducing grid burden and energy operating cost in the future. The promising benefits of energy flexibility and cost efficiency of the proposed building-vehicle energy network will promote the development of H_2 infrastructure which will help actualize regional carbon neutralization.

(3) The parametric study on the effects of the increased HV quantity and the decreased renewable price sheds some

lights on the development of building-vehicle energy networks in the near future. To be specific, Sections 3.2 and 3.3 indicate that with the increased HV quantity, the vehicle-related cost (the H_2 cost for daily transportation and the fuel cell degradation cost), rather than the grid cost by buildings, will be the main cost sector of regional energy networks. Furthermore, with the decreased economic incentives in renewable energy, exporting renewable electricity to the local grid will be less cost-efficient than being shared in vehicles via the V2G interactions. The benefits of transferring surplus renewables from buildings to vehicles shown in this paper provides the promising solution for actualizing carbon-neutral and low-cost communities in the future.

Meanwhile, the limitations herein are clarified for further improvements of future studies:

(1) California's climate is moderate throughout the whole year, which leads to the low HVAC energy consumptions of both buildings and vehicles. Also, the vehicle PEMFCs are in relative moderate environments, rather than extremely hot or cold environments. Therefore, the results of this study are more proper for regions with moderate climates. Future studies should be extended to regions with various climates for exploring the performance of the proposed building-vehicle energy networks.

(2) The cabin thermal model and the fuel cell degradation model developed in this study provide practical methods of analyzing the working environment and degradation of vehicle PEMFCs with a relatively high computation efficiency. Nonetheless, the models are simplified and some key parameters are obtained from previous studies. Future studies are still needed for more advanced and accurate models, together with parameters for the practical application of the building-vehicle energy networks.

(3) For now, California's H_2 infrastructure is still under development, and there are no economic policies for the energy trade between H_2 stations and the adjacent buildings or communities. Therefore, this study determines the final H_2 cost according to the net H_2 consumption by the community, and does not include the cost of hot water provided by the H_2 station. In practice, a detailed energy trade between H_2 stations and the adjacent buildings or communities might include the maintenance costs of the onsite H_2 system (such as the electrolyzer and compressor) and hot water systems at the H_2 station. Therefore, the actual energy operating cost should be investigated with different energy trading policies in the future studies.

(4) This study only investigates a residential community within one year, and the corresponding fuel degradation is small within such a short term. Other buildings, like office buildings, with different energy consumption characteristics from residential buildings, might cause different levels of fuel cell degradation in building-vehicle energy networks. The influences of different building types, increased building quantities, and other factors will be added and explored in our future studies. The decreased fuel cell efficiency might exert significant effects on the whole energy network in the long run after the accumulated fuel cell degradation reaches a relative level like 10%. The long-term performance change, such as 20 years [61], will be investigated in our future studies.

(5) In the investigated community, the H_2 station is the only place of storing the PV electricity-generated H_2. Nonetheless, the overall electricity-H_2-electricity conversion efficiency is 40-50%, leading to a relatively high energy loss for the whole energy network. In order to improve the network energy efficiency, multiple energy storages with a high energy efficiency are needed, such as electrochemical batteries for electricity storage and grid interaction [62, 63]. Integrating synergistic energy storages in building-vehicle energy networks will be explored in our future work.

5 Conclusions

Deploying H_2-based building-vehicle energy networks is an effective strategy to improve intermittent renewable penetration, enhance regional energy flexibility and reduce the reliance on fossil fuels, where vehicle PEMFCs are the key components to actualize the gas-to-power conversion for clean power supply. However, the vehicle PEMFCs suffer from performance degradation, dependent on the cabin heat balance and power requirements during the transportation

and V2G interaction procedures, but this issue is seldomly explored in the current academia. This study firstly proposes a two-space cabin thermal model for calculating (1) the cabin indoor temperature to which vehicle PEMFCs are exposed and (2) the energy consumption of vehicle HVAC systems supported by PEMFCs. Afterwards, based on a previous study [30], a fuel cell stack voltage model is proposed to quantify the performance degradation magnitude of vehicle PEMFCs for daily transportation and V2G interactions, respectively. Moreover, these two models are coupled with a community-level electricity-H_2 hybrid building-vehicle energy network in California, U.S.A. The community integrates low-rise single houses, rooftop PV systems, HVs, a H_2 station, community micro power grid, local power grid, and local H_2 pipelines. This building-vehicle network also formulates multiple energy interactions among the buildings, HVs, and H_2 station for improving energy flexibility and grid stability. In order to highlight the necessity for fuel cell degradation and to avoid the techno-economic performance overestimation, grid interaction, fuel cell degradation, and energy operating cost of the proposed building-vehicle energy network are evaluated in the cases with and without considering the fuel cell degradation. Furthermore, the potential effects of fuel cell degradation on the district energy network are evaluated with the increased HV quantity and the decreased renewable electricity price. Main conclusions of this study are listed as follows:

(1) The renewable congestion and demand shortage can be effectively ameliorated with the integration of H_2 station and V2G interactions in the community. About 75% of the annual renewable electricity is absorbed by the electrolyzer and compressor at the H_2 station, covering about 28% of the community's annual energy demand. Furthermore, the fuel cell degradation does not obviously affect the grid stability, due to the limited fuel cell degradation in the short term.

(2) In the proposed building-vehicle energy network, the fuel cell degradation is 3.16% per vehicle within one year, where 2.50% and 0.66% are caused by daily transportation and V2G interactions, respectively. Namely, the V2G interaction increases the fuel cell degradation rate by 26.4% as compared to the condition when vehicle PEMFCs are only used to support transportation energy demand. This result highlights the importance of fuel cell degradation to avoid the overestimation on dynamic and lifetime performance analysis.

(3) The fuel cell degradation accounts for a considerable proportion of the total energy cost. In the proposed building-vehicle energy network, the total fuel cell degradation cost is $6945.2, reaching 33.4% of the total operating cost ($20770.61). If the fuel cell degradation is not considered (Case 1), the energy operating cost of the building-vehicle energy network will be underestimated by about 37%.

(4) The increased HV quantity integrated in the community reduces fuel cell degradation magnitude for each HV in V2G interactions. When the HV quantity increases from four to twenty, the fuel cell degradation by V2G interactions decreases from 0.66% to 0. Correspondingly, when the HV quantity increases from four to twenty, the total fuel cell degradation of each HV decreases from 3.16% to 2.50%. Moreover, when the HV quantity increases from four to twenty, the grid cost, H_2 cost, and fuel cell degradation cost of the building-vehicle network increase from $15675.6 to $32438.9, from -$1850.1 to $4315.1, and from $6945.2 to $27524.6, respectively. Correspondingly, the total operating cost increases from $20770.6 to $64278.6, by over 200%. The proportion of the fuel cell degradation cost to total operating cost increases from 33.4% to 42.8%. If the fuel cell degradation is not considered (Case 1), as the HV quantity increases from four to twenty, the energy operating cost will be underestimated by 37%-44%, which indicates the significance and necessity of fuel cell degradation to avoid the economic performance overestimation of building-vehicle energy networks.

(5) The decreased renewable electricity price in the future will necessitate the V2G interactions to improve the economic competitiveness of the building-vehicle energy network. To be specific, in the proposed building-vehicle energy network (Case 2), when the decreasing magnitude of renewable electricity price increases from 0 to 100%, the grid cost increases from $15675.6 to $19843.5, resulting in the increase of total operating cost from $20770.6 to

$24938.5. Correspondingly, the proportion of fuel cell degradation cost to the total operating cost decreases from 33.4% to 27.8%. Such a finding indicates that the fuel cell degradation cost is still an essential part in the building-vehicle network with the decreased renewable price. Moreover, if the reference case with isolated buildings and HVs also considers the fuel cell degradation caused by daily transportation, the energy operating cost of Case 2 (with V2G interactions and fuel cell degradation) is lower than that of the reference case when the renewable electricity price is reduced by 40% or more. In other words, the cost saving by deploying V2G interactions can compensate the fuel cell degradation cost when the renewable electricity price of California is reduced by 40% or more.

Acknowledgments

This study is supported by the funding of Center for the Built Environment, University of California, Berkeley (Number: 59297 24003 44). This research is also supported by Hunan University and Hong Kong Polytechnic University. All copyright licenses have been successfully applied for all cited graphics, images, tables and/or figures.

References

[1] He Y, Li N, Li N, Li J, Yan J, Tan C. Control behaviors and thermal comfort in a shared room with desk fans and adjustable thermostat. Build Environ. 2018;136:213-26.
[2] He Y, Li N, Zhang H, Han Y, Lu J, Zhou L. Air-conditioning use behaviors when elevated air movement is available. Energy Build. 2020:110370.
[3] He Y, Li N, Lu J, Li N, Deng Q, Tan C, et al. Meeting thermal needs of occupants in shared space with an adjustable thermostat and local heating in winter: An experimental study. Energy Build. 2021;236:110776.
[4] Zhou Y, Cao S, Hensen JL, Lund PD. Energy integration and interaction between buildings and vehicles: A state-of-the-art review. Renewable and Sustainable Energy Reviews. 2019;114:109337.
[5] Zhou Y, Cao S, Hensen JL. An energy paradigm transition framework from negative towards positive district energy sharing networks—Battery cycling aging, advanced battery management strategies, flexible vehicles-to-buildings interactions, uncertainty and sensitivity analysis. Applied Energy. 2021;288:116606.
[6] Administration USEI. U.S. energy facts explained. https://www.eia.gov/energyexplained/us-energy-facts/ (2020).
[7] Agency EE. Final energy consumption by sector. http://www.eea.europa.eu/data-andmaps/daviz/total-final-energy-consumption-by-sector-1#tab-chart_3 (2015).
[8] Farahani SS, Bleeker C, van Wijk A, Lukszo Z. Hydrogen-based integrated energy and mobility system for a real-life office environment. Applied Energy. 2020;264:114695.
[9] Firtina-Ertis I, Acar C, Erturk E. Optimal sizing design of an isolated stand-alone hybrid wind-hydrogen system for a zero-energy house. Applied Energy. 2020;274:115244.
[10] Liu J, Cao S, Chen X, Yang H, Peng J. Energy planning of renewable applications in high-rise residential buildings integrating battery and hydrogen vehicle storage. Applied Energy. 2021;281:116038.
[11] Liu J, Chen X, Yang H, Shan K. Hybrid renewable energy applications in zero-energy buildings and communities integrating battery and hydrogen vehicle storage. Applied Energy. 2021;290:116733.
[12] Abdin Z, Zafaranloo A, Rafiee A, Mérida W, Lipiński W, Khalilpour KR. Hydrogen as an energy vector. Renewable and Sustainable Energy Reviews. 2020;120:109620.
[13] Corporation TM. Toyota Ushers in the Future with Launch of 'Mirai' Fuel Cell Sedan. www.toyota-global.com/innovation/environmental_technology/fuelcell_vehicle/
[14] Co. HM. 2020 Honda CLARITY Fuel Cell. https://automobiles.honda.com/clarity-fuel-cell (2020).
[15] Lux B, Pfluger B. A supply curve of electricity-based hydrogen in a decarbonized European energy system in 2050. Applied Energy. 2020;269:115011.
[16] Navas-Anguita Z, García-Gusano D, Dufour J, Iribarren D. Prospective techno-economic and environmental assessment of a national hydrogen production mix for road transport. Applied Energy. 2020;259:114121.
[17] Szima S, Nazir SM, Cloete S, Amini S, Fogarasi S, Cormos A-M, et al. Gas switching reforming for flexible power and hydrogen production to balance variable renewables. Renewable and Sustainable Energy Reviews. 2019;110:207-19.
[18] Gabrielli P, Poluzzi A, Kramer GJ, Spiers C, Mazzotti M, Gazzani M. Seasonal energy storage for zero-emissions multi-energy systems via underground hydrogen storage. Renewable and Sustainable Energy Reviews. 2020;121:109629.
[19] Mehrjerdi H, Bornapour M, Hemmati R, Ghiasi SMS. Unified energy management and load control in building equipped with wind-solar-battery incorporating electric and hydrogen vehicles under both connected to the grid and islanding modes. Energy. 2019;168:919-30.
[20] Cao S, Alanne K. Technical feasibility of a hybrid on-site H2 and renewable energy system for a zero-energy building with a H2 vehicle. Applied Energy. 2015;158:568-83.

[21] Sahu AV, Lee EHP, Lukszo Z. Exploring the potential of the vehicle-to-grid service in a sustainable smart city. 2018 IEEE 15th International Conference on Networking, Sensing and Control (ICNSC): IEEE; 2018. p. 1-6.
[22] Maroufmashat A, Fowler M, Khavas SS, Elkamel A, Roshandel R, Hajimiragha A. Mixed integer linear programing based approach for optimal planning and operation of a smart urban energy network to support the hydrogen economy. International Journal of hydrogen energy. 2016;41:7700-16.
[23] Mukherjee U, Maroufmashat A, Ranisau J, Barbouti M, Trainor A, Juthani N, et al. Techno-economic, environmental, and safety assessment of hydrogen powered community microgrids; case study in Canada. International Journal of Hydrogen Energy. 2017;42:14333-49.
[24] Felgenhauer MF, Pellow MA, Benson SM, Hamacher T. Evaluating co-benefits of battery and fuel cell vehicles in a community in California. Energy. 2016;114:360-8.
[25] Oldenbroek V, Verhoef LA, Van Wijk AJ. Fuel cell electric vehicle as a power plant: Fully renewable integrated transport and energy system design and analysis for smart city areas. International Journal of Hydrogen Energy. 2017;42:8166-96.
[26] Lin R-H, Zhao Y-Y, Wu B-D. Toward a hydrogen society: Hydrogen and smart grid integration. International Journal of Hydrogen Energy. 2020;45:20164-75.
[27] Association FCHE. Road Map to a US Hydrogen Economy http://www.fchea.org/us-hydrogen-study (2020).
[28] Das HS, Tan CW, Yatim A. Fuel cell hybrid electric vehicles: A review on power conditioning units and topologies. Renewable and Sustainable Energy Reviews. 2017;76:268-91.
[29] Yue M, Jemei S, Gouriveau R, Zerhouni N. Review on health-conscious energy management strategies for fuel cell hybrid electric vehicles: Degradation models and strategies. International Journal of Hydrogen Energy. 2019;44:6844-61.
[30] Pei P, Chang Q, Tang T. A quick evaluating method for automotive fuel cell lifetime. International Journal of Hydrogen Energy. 2008;33:3829-36.
[31] Petrone R, Zheng Z, Hissel D, Péra M-C, Pianese C, Sorrentino M, et al. A review on model-based diagnosis methodologies for PEMFCs. International Journal of Hydrogen Energy. 2013;38:7077-91.
[32] Cadet C, Jemeï S, Druart F, Hissel D. Diagnostic tools for PEMFCs: from conception to implementation. International Journal of Hydrogen Energy. 2014;39:10613-26.
[33] Polverino P, Bove G, Sorrentino M, Pianese C, Beretta D. Advancements on scaling-up simulation of Proton Exchange Membrane Fuel Cells impedance through Buckingham Pi theorem. Applied energy. 2019;249:245-52.
[34] Morando S, Jemei S, Gouriveau R, Zerhouni N, Hissel D. Fuel cells prognostics using echo state network. IECON 2013-39th Annual Conference of the IEEE Industrial Electronics Society: IEEE; 2013. p. 1632-7.
[35] Silva R, Gouriveau R, Jemei S, Hissel D, Boulon L, Agbossou K, et al. Proton exchange membrane fuel cell degradation prediction based on adaptive neuro-fuzzy inference systems. International Journal of Hydrogen Energy. 2014;39:11128-44.
[36] Li H, Ravey A, N'Diaye A, Djerdir A. Equivalent consumption minimization strategy for fuel cell hybrid electric vehicle considering fuel cell degradation. 2017 IEEE transportation electrification conference and expo (ITEC): IEEE; 2017. p. 540-4.
[37] Ozden E, Tari I. PEM fuel cell degradation effects on the performance of a stand-alone solar energy system. International Journal of Hydrogen Energy. 2017;42:13217-25.
[38] Tajitsu N, Shiraki M. Toyota plans to expand production, shrink cost of hydrogen fuel cell vehicles. https://www.reuters.com/article/us-toyota-hydrogen-idUSKBN1KG0Y0 (2018).
[39] Pyrgou A, Kylili A, Fokaides PA. The future of the Feed-in Tariff (FiT) scheme in Europe: The case of photovoltaics. Energy Policy. 2016;95:94-102.
[40] Commission CE. Tracking Progress of Renewable Energy. https://www.energy.ca.gov/sites/default/files/2019-12/renewable_ada.pdf (2020).
[41] Partnership CFC. FCEV Sales, FCEB, & Hydrogen Station Data. https://cafcp.org/by_the_numbers (2020).
[42] Partnership CFC. The California Fuel Cell Revolution (CaFCP). https://cafcp.org/sites/default/files/CAFCR.pdf (2018).
[43] He Y, Zhou Y, Yuan J, Liu Z, Wang Z, Zhang G. Transformation towards a carbon-neutral residential community in California, U.S.A., with hydrogen economy and advanced energy management strategies--distributed renewable power supply, fuel-cell vehicles, hydrogen stations, and power grid. Submitted to Energy Conversion and Management.
[44] Standard A. Standard 90.2-2018 “Energy-Efficient Design of Low-Rise Residential Buildings”. American Society of Heating, Refrigerating and Air-Conditioning Engineers, Inc Atlanta, GA, USA. 2018.
[45] Parker DS, Fairey PW, Lutz JD. Estimating daily domestic hot-water use in North American homes. ASHRAE Trans. 2015;121.
[46] CA 2007 Plumbing Code, Chapter 4. https://inspectapedia.com/plumbing/California_Plumbing_Code_Ch04.pdf (2000).
[47] NeON® R ACe Solar Panels. https://www.lg.com/us/business/download/resources/CT00002151/LG370-380A1C-V5_PRE_FinalVer_083019[20190921_023718].pdf
[48] Company PGaE. ELECTRIC SCHEDULE E-TOU-D. https://www.pge.com/tariffs/assets/pdf/tariffbook/ELEC_SCHEDS_E-TOU-D.pdf (2020).
[49] Company PGaE. Understand Net Energy Metering and your bill. https://www.pge.com/en_US/residential/solar-

and-vehicles/green-energy-incentives/solar-and-renewable-metering-and-billing/net-energy-metering-program-tracking/understand-net-energy-metering.page (2020).
[50] Company PGaE. Getting credit for surplus energy. https://www.pge.com/en_US/residential/solar-and-vehicles/green-energy-incentives/getting-credit-for-surplus-energy/getting-credit-for-surplus-energy.page (2020).
[51] Partnership CFC. Cost to refill. https://cafcp.org/content/cost-refill (2020).
[52] 2016 Toyota Mirai 4dr Sdn Features And Specs. https://www.caranddriver.com/toyota/mirai/specs/2016/toyota_mirai_toyota-mirai_2016
[53] Hou Y, Wan G, Jiang W, Zhuang M. Properties Analysis of Hydrogen Consumption Rate for a PEM Fuel Cell Engine. SAE Technical Paper; 2006.
[54] Lohse-Busch H, Stutenberg K, Duoba M, Iliev S. Technology assessment of a fuel cell vehicle: 2017 Toyota Mirai. Argonne National Lab.(ANL), Argonne, IL (United States); 2018.
[55] Neubauer J, Wood E. Thru-life impacts of driver aggression, climate, cabin thermal management, and battery thermal management on battery electric vehicle utility. Journal of Power Sources. 2014;259:262-75.
[56] Ott W, Klepeis N, Switzer P. Air change rates of motor vehicles and in-vehicle pollutant concentrations from secondhand smoke. Journal of exposure science & environmental epidemiology. 2008;18:312-25.
[57] Fayazbakhsh MA, Bahrami M. Comprehensive modeling of vehicle air conditioning loads using heat balance method. SAE technical paper. 2013;2013:1507.
[58] He Y, Arens E, Li N, Wang Z, Zhang H, A Y, et al. Modeling solar radiation on a human body indoors by a novel mathematical model. Build Environ. 2021;187:107421.
[59] Marcos D, Pino FJ, Bordons C, Guerra JJ. The development and validation of a thermal model for the cabin of a vehicle. Applied Thermal Engineering. 2014;66:646-56.
[60] A TRANSIENT SYSTEMs Simulation Program. Mechanical Engineering Department, UW Madison. https://sel.me.wisc.edu/trnsys/ (2017).
[61] Zhou Y, Cao S. Coordinated multi-criteria framework for cycling aging-based battery storage management strategies for positive building–vehicle system with renewable depreciation: Life-cycle based techno-economic feasibility study. Energy Conversion and Management. 2020;226:113473.
[62] Zhou Y, Cao S. Energy flexibility investigation of advanced grid-responsive energy control strategies with the static battery and electric vehicles: A case study of a high-rise office building in Hong Kong. Energy Conversion and Management. 2019;199:111888.
[63] Zhou Y, Cao S, Hensen JL, Hasan A. Heuristic battery-protective strategy for energy management of an interactive renewables–buildings–vehicles energy sharing network with high energy flexibility. Energy Conversion and Management. 2020;214:112891.